

Analogy of Gold, Silver, Copper and Aluminium Based Ultra-Sensitive Surface Plasmon Resonance Photonic Crystal Fibre Biosensors

A DISSERTATION

SUBMITTED IN PARTIAL FULFILLMENT OF THE
REQUIREMENTS FOR THE AWARD OF THE DEGREE

OF

MASTER OF SCIENCE

IN

PHYSICS

Submitted by:

MADHUR

2K21/MSCPHY/27

Under the supervision of

PROF. VINOD SINGH



DEPARTMENT OF APPLIED PHYSICS
DELHI TECHNOLOGICAL UNIVERSITY
(Formerly Delhi college of Engineering)

Bawana road, Delhi-110042

DELHI TECHNOLOGICAL UNIVERSITY
(Formerly Delhi College of Engineering)
Bawana road, Delhi-110042

CANDIDATE'S DECLARATION

I, **Madhur** (2K21/MSCPHY/27) student of M.Sc. physics, hereby declare that the project dissertation titled “**Analogy of Gold, Silver, Aluminium, Copper based Ultra Sensitive Surface Plasmon Resonance Photonic Crystal Fibre Biosensors**” which is submitted by me to the Department of Applied Physics, Delhi Technological University, Delhi. In partial fulfilment of the requirement for the award of the degree of Master of Science, is originally and not copied from any source without proper citation. This work has not previously formed the basis for the award of any Degree, Fellowship or other similar title or recognition. The work has been accepted/communicated in SCI/SCI expanded/SSCI/ Scopus indexed journal or Peer-reviewed Scopus indexed conference with the following details:

TITLE OF THE PAPER: Analogy of Gold, Silver, Aluminium, Copper based Ultra Sensitive Surface Plasmon Resonance Photonic Crystal Fibre Biosensors.

Author Names: Madhur, Deepak kumar, Mukta Sharma, Vinod Singh

Name of the conference: ICMMS2022- 1st International Conference on Materials and Manufacturing for Sustainable Development (**ICMMS-2022**), Department of Mechanical Engineering SRMUH Delhi-NCR

Conference date: 16th September, 2022

Status of paper: Published

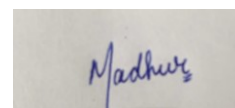
Publishing Journal: Materials Today Proceedings, Elsevier

Date of paper Acceptance: 30 August, 2022

Date of paper publication: 2 March 2023

Date of paper available online: 6 March 2023

Have you attend the conference (YES/NO): Yes



MADHUR
(2K21/MSCPHY/27)

SUPERVISOR CERTIFICATE

To the best of my knowledge, the above work has not been submitted in part or full for any Degree or Diploma to this University or elsewhere. I, further certify that the publication and indexing information given by the student is correct.



Place: New Delhi

Date: 31-May-2023

PROF. VINOD SINGH

Supervisor

CERTIFICATE

I, hereby certify that the project dissertation titled “Analogy of Gold, Silver, Copper and Aluminium Based Ultra-Sensitive Surface Plasmon Resonance Photonic Crystal Fibre Biosensors”, by Madhur (2K21/MSCPHY/27) submitted to the Department of Applied Physics, Delhi Technological University in partial fulfilment of the requirement for the award of the degree of Master of Science, is a record of the project work carried out by student under my supervision. This work has not been submitted partially or completely during any degree or diploma to this university or anywhere else, to the best of my knowledge.



Place: New Delhi

Date: 31-May-2023

PROF. VINOD SINGH

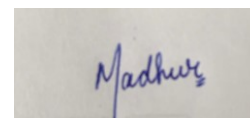
Supervisor

ABSTRACT

Biosensors have become increasingly utilised in the medical and pharmaceutical fields in recent years. Surface Plasmon Resonance is one of the most often exploited phenomenon for the development of biosensors. Typically, optical fibres are used to create biosensors. However, the sensing properties are much improved when photonic crystal fibres are used in place of optical fibres. In these sensors, an air-holed surface is encircled by a thin nano-film of plasmonic metals, including gold, silver, copper, and aluminium, as well as the plasmonic metal alloy gold-tin, which is filled with an appropriate analyte. Designing an internal type PCF sensor with analyte and several micrometer-sized holes in the centre is the main goal of this paper. One by one, the properties of the various plasmonic materials are examined. Each plasmonic material's amplitude and wavelength sensitivity are calculated. Copper, silver, gold, and aluminium all have wavelength sensitivities of 1799nmRIU^{-1} , 1830.76nmRIU^{-1} , 1732nmRIU^{-1} , and 1652nm/RIU , respectively. The predicted wavelength sensitivity for the Gold-Tin alloy is 1532.2nmRIU^{-1} . The characteristics of these various sensors are then contrasted. The best results are seen for gold with the same set of settings, but the thickness of the gold layer cannot be decreased to a few nanometers. Thus, silver has been found to be the best suitable metal in terms of stability and a wide variety of criteria.

ACKNOWLEDGMENT

I would like to express my indebtedness and deepest sense of regard to my supervisor, PROF. VINOD SINGH, Department of Applied Physics, Delhi Technological University for providing his incessant expertise, inspiration, encouragement, suggestions and this opportunity to work under his guidance. I am grateful for the constant help provided at every step of this project by all the lab members, Department of Applied Physics, Delhi Technological University. I am also thankful to my family and colleagues for their invaluable support, care and patience during this project. Lastly, I would thank Delhi Technological University for providing such a wonderful opportunity of working on this project.

A rectangular box containing a handwritten signature in blue ink that reads "Madhur".

MADHUR
(2K21/MSCPHY/27)

CONTENTS

CANDIDATE'S DECLARATION	ii-iii
CERTIFICATE	iv
ABSTRACT	v
ACKNOWLEDGEMENT	vi
CONTENTS	vii-viii
TABLE OF FIGURES	ix
LIST OF TABLES	x
LIST OF SYMBOLS, ABBREVIATIONS	x
CHAPTER 1: INTRODUCTION	1-10
1.1 BIOSENSORS	
1.2 SURFACE PLASMON RESONANCE	
1.3 PHOTONIC CRYSTAL FIBER	
1.4 PHOTONIC CRYSTAL FIBER BASED SURFACE PLASMON RESONANCE	
1.5 OBJECTIVE OF STUDY	
CHAPTER 2: METHODOLOGY	11-13
2.1 NUMERICAL MODEL	
2.2 SIMULATION MODEL	

CHAPTER 3: DESIGN AND MODELLING	14-16
3.1 STRUCTURAL DESIGN	
CHAPTER 4: RESULTS AND DISCUSSION	17-25
4.1 PHASE MATCHING	
4.2 CALCULATION OF WAVELENGTH SENSITIVITIES	
4.3 CALCULATION OF AMPLITUDE SENSITIVITIES	
CHAPTER 5: COMPARISON OF DIFFERENT PHOTONIC CRYSTAL FIBER	26-28
CHAPTER 6: SUMMARY	29
CHAPTER 7: FUTURE WORK	30
REFERENCES	31-33
APPENDICES:	
APPENDIX 1: PLAGIARISM REPORT	34-35
APPENDIX 2: ABSTRACT ACCEPTANCE	36
APPENDIX 3: CONFERENCE CERTIFICATE	36
APPENDIX 4: PROOF OF SCOPUS INDEXIN	37
APPENDIX 5: PAPER ACCEPTANCE	37
APPENDIX 6: FULL RESEARCH PAPER	38-43

TABLE OF FIGURES

Figure No.	Title	Page No.
Figure 1.1	Important components of Biosensors	2
Figure 1.2	Representation of Surface Plasmon Resonance	3
Figure 1.3	Intensity dip in surface plasmon curve	2
Figure 1.4	Geometrical representation of the different types of PCFs	7
Figure 1.5	Advantages of PCF SPR sensors	10
Figure 3.1	Desired sensor model is depicted schematically	15
Figure 3.2	Model structure in COMSOL	16
Figure 4.1 (a)	Core mode neff	17
Figure 4.1 (b)	SPP mode neff	17
Figure 4.2	Core and SPP mode phase matching curve for gold nanofilm	18
Figure 4.3	Core and SPP mode phase matching curve for silver nanofilm	19
Figure 4.4	Curve of Confinement loss for gold nanofilm ($n_a=1.25-1.30$)	19
Figure 4.5	Curve of Confinement loss for silver nanofilm ($n_a=1.25-1.30$)	20
Figure 4.6	Curve of Confinement loss for aluminium nanofilm ($n_a=1.25-1.30$)	20
Figure 4.7	Curve of Confinement loss for copper nanofilm ($n_a=1.25-1.30$)	21
Figure 4.8	Curve of Confinement loss for gold-tin alloy nanofilm ($n_a=1.25-1.30$)	21
Figure 4.9	Amplitude sensitivity curve for gold nanofilm ($n_a=1.25-1.30$)	23
Figure 4.10	Amplitude sensitivity curve for silver nanofilm ($n_a=1.25-1.30$)	23
Figure 4.11	Amplitude sensitivity curve for aluminium nanofilm ($n_a=1.25-1.30$)	24
Figure 4.12	Amplitude sensitivity curve for copper nanofilm ($n_a=1.25-1.30$)	24
Figure 4.13	Amplitude sensitivity curve for gold-tin alloy nanofilm ($n_a=1.25-1.30$)	24

LIST OF TABLES

Table 1: Wavelength sensitivities for different materials

LIST OF SYMBOLS & ABBREVIATIONS

SPR- Surface Plasmon Resonance

PCF- Photonic Crystal Fibre

SPP- Surface Plasmon Polariton

SPW- Surface Plasmonic Waves

FEM- Finite Element Method

TIR- Total Internal Reflection

DL -Drude-Lorentz

CHAPTER 1

INTRODUCTION

1.1 BIOSENSORS:

An analytical tool called a biosensor contains immobilised biological components (such as enzymes or antibodies) that, when in contact with an analyte, modify the analyte physically, chemically, or electrically and produce a signal that may be detected. Biosensors are those which convert biological response to electric signal. Biological analytes including biomolecular biological structures and bacteria can be detected by biosensors along with their concentration [1]. The physical and chemical changes brought about by this interaction are recognised by the transducer and translated into an electrical signal. Analyte concentration in the sample is determined by interpreting and converting this signal. The knock-on effect occurs in optical biosensors when any analyte or molecule is detected; this action can cause light to be absorbed or to be emitted. Therefore, we can quantify this released light using optical biosensors [1]. Basic examples are thermometer, stethoscope and ECG machine. Analyte whose concentration to be measured contact with bio-receptor gives signal and output is measurable. Biosensors are based on the principle of signal transduction. The advantages of Biosensors are their fast response time, rapid and continuous measurement.

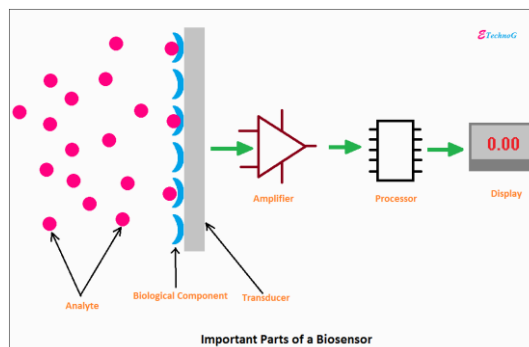


Figure 1.1: Important components of biosensors

Image courtesy: etechnog.com

Biosensors are made up of a bio-element, a transducer, an amplifier, a processor, and an output display device. There are many different kinds of biosensors, some of which include conductometric, electrochemical, potentiometer biosensors and thermometric biosensors, SPR biosensors have been used in many significant domains, such as safety related to food and security, monitoring the environment, and medical evaluations [2].

1.2 SURFACE PLASMON RESONANCE :

For the investigation of label-free bio-molecular interaction, it is a potent detection method. The resonance angle is the angle at which light from the light source, which is passing through a prism, reflects off the back of the sensorship and enters a detector.

Plasmon resonance at the surface (SPR) is a phenomenon that happens when p-polarized or transverse magnetic light strikes a surface. This incident light causes the electrons on the surface to oscillate the plasmonic Surface Waves. The metal-dielectric medium interaction is where SPW are produced [3]. Electrons in the sensor

chip's metal sheet absorb light, which makes them vibrate and make them susceptible to their surroundings.

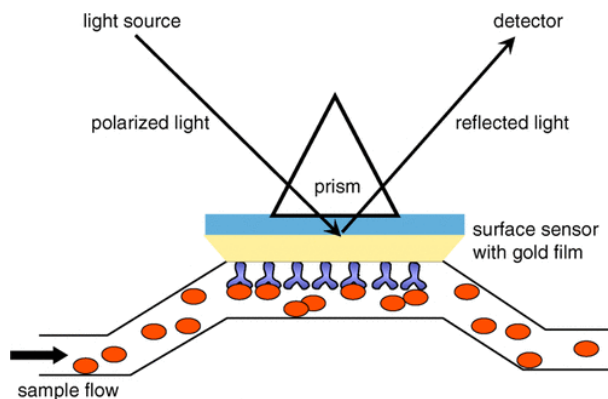


Figure 1.2: Representation of surface plasmon resonance

Image courtesy: thesciencenotes.com/

Under specific circumstances, the coupling of the EM waves incident on the surface with the SPW and Total internal reflection results in the SPR [4].

This result can be identified as a dip in the SPR reflection curve because it appears as a black band in the beam being reflected, which can be utilised to communicate details about the sensor surface.

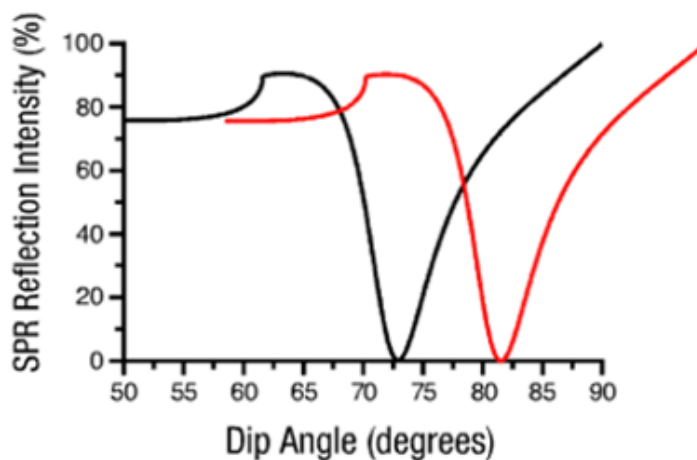


Figure 1.3: Intensity dip in surface plasmon curve

Image courtesy: biosensingusa.com

Technology is frequently used to explore the interactions between probe molecules that immobilise on the sensor surface and free analyte molecules in solution. The angular position of the black band moves when molecular binding occurs, and a shift in the reflectivity curve can also be seen. It gauges changes in the medium's refractive index that come into direct contact with the sensor surface. Aqueous samples containing analyte proteins are frequently the surface's medium of contact. After some of the refracted light is absorbed, a dark region appears in the refracted light coming from the detector. Despite a constant angle of incidence, the incident light's wavelength changes. Then, at a specific the incident light's wavelength, a strong peak is seen, signifying the achievement of SPR [5]. Because of the energy that is absorbed, the electrons in metal begin to oscillate, and a group of electrons that have collectively absorbed energy are known as plasmons. At specific metal contacts, a special type of electromagnetic wave known as a plasmon can be excited.

SPR-based sensors primarily make use of the idea of the metal-dielectric contact surface's electron being excited. When a specific wavelength and angle of incidence allow for phase matching. Corresponding variation in the Surface Plasmon Waves' refractive index values is noticed. Factors that affect SPR are:

- The light's incident wave length
- Incidence angle
- The metal's and the dielectric's respective dielectric constants

The values of the incidence angle and the incident light's wavelength are determined. by the values of the dielectric constant of the media that we utilise [4]. Spectral interrogation is the procedure used to determine the wavelength at which a substance exhibits SPR [6]. The change in the excited electrons' wavelength has been found to correspond to rising

in the refractive index exponentially, which else enables the determination of the precise incident light wavelengths. The SPR-based sensors have many benefits, including label-free detection—which eliminates the need for time-consuming or expensive labelling protocols—rapid response, measurements of analyte binding, effective light-controlling capabilities and for the time being, true quantity detection. Gold, silver, and aluminium are the most prevalent plasmonic materials.

These materials are grouped with copper, gold-tin alloy, and niobium nanofilm as plasmonic materials [5].

1.2.1 PRINCIPLE OF SPR:

The SPR phenomenon operates according to the Surface Plasma oscillations theory.

Electron oscillations are attained along the surface as well as the metal-dielectric contact, and the quantum of oscillating electrons at the surface is referred to as a plasmon [7].

Both the metal and the dielectric exhibit this exponential decline. By resolving equations from Maxwell's theory of electromagnetism with conditions governing the boundary surface and the metal and dielectric portions taken separately, it is possible to calculate the polarisation of the component known as the transverse magnetic field and the exponential decay in the electric field [8]. Fano's reasoning led to the conclusion that the electromagnetic waves impacting on the diffraction grating surface were what excited the electrons [9]. Additionally, the SPR-based sensors are well renowned for their accuracy and precision in detecting even the smallest changes in the metal interface that is commonly employed as the analyte for the SPR-based sensor as well as the dielectric medium's refractive index.

1.3 PHOTONIC CRYSTAL FIBER:

PCF is referred to as “HOLEY FIBER” because of the presence of air gaps. It is microstructured fiber. In order to achieve the SPR condition, a class of optical fibres are called photonic crystal fibres (PCF) that primarily utilise plasmonic crystals in and around their core. PCF is essentially an optical fibre with background materials with a low regular arrangement of refractive index. The PCFs are constructed with several of many air holes that span the extent of the fibre in order to provide a low loss dielectric-based fibre. Modified total internal reflection in addition to photonic band gap guiding can be used to direct light inside the PCF. Due to the presence of photonic crystals, the purpose of PCF is to prevent the propagation of light with a specific wavelength in a particular direction.

The PCF is based on the TIR phenomenon, which aids in the forward motion of the light wave through the core. The cladding and inner core components of optical fibres always have a lower refractive index than PCFs, which can vary. Because air holes are present, cladding refraction is lower than core refraction.

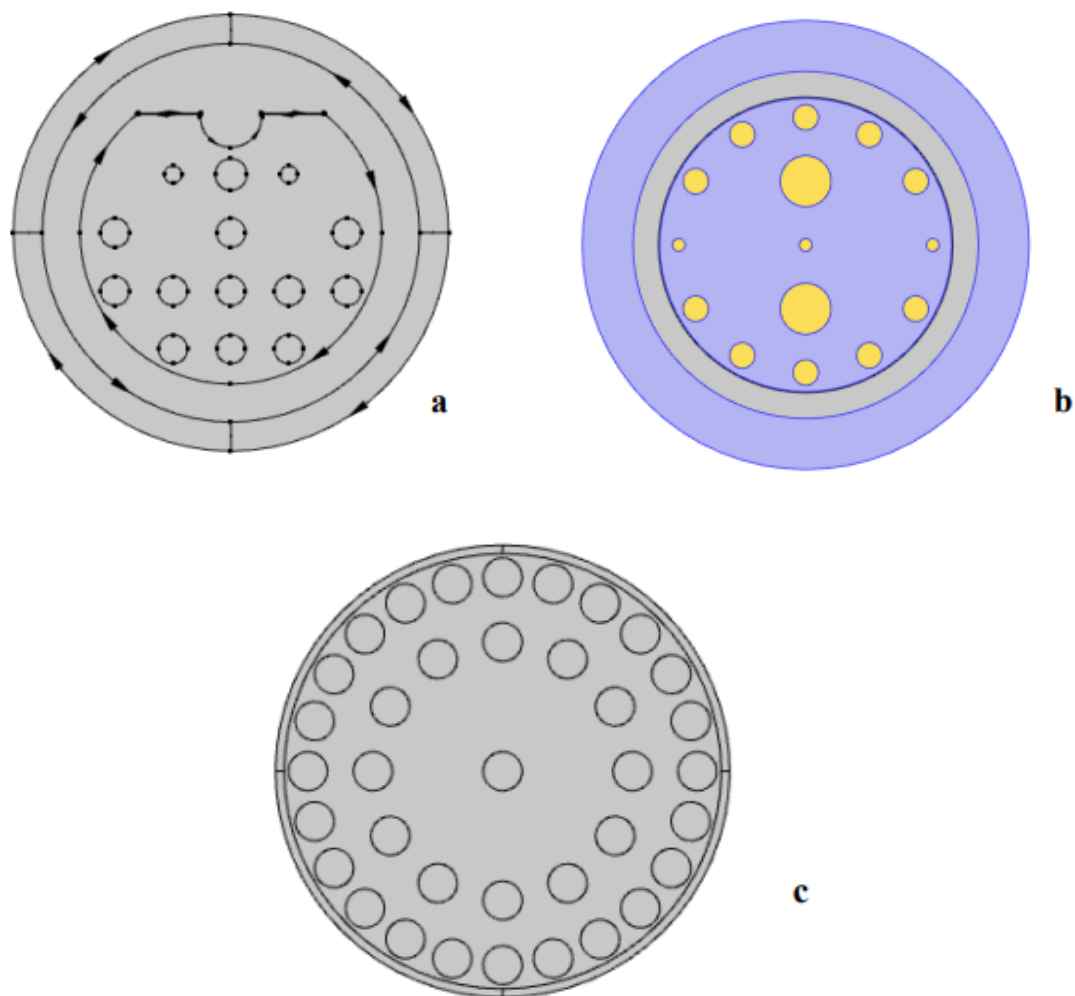


Figure 1.4. The geometrical representation of the different types of PCFs. (a) D-shaped PCF sensor with multiple holes filled with and a layer of plasmonic material nanofilm around the D- curve. (b) PCF containing two cores along with a multiple air hole structure with holes of varying diameters. (c) Single-core PCF structure with a core at the middle and the cladding with holes of the same diameter.

1.3.1 PCF'S BENEFITS OVER OPTICAL FIBRES:

Because of their microstructure, micro-structured fibres offer a unique versatility for modifying their characteristics and guidance capabilities. Total internal reflection is followed by the construction of traditional optical fibres, which consists of a core and cladding. In PCF, however, the multicore structure uses improvised total internal

reflection based on the photonic band-gap. Additionally, the presence of holes can be used to enhance the fiber's capacity for sensing by enhancing the interactivity between the measurement the light and the analyzer travelling through it. The most flexible, symmetrical, and evanescent structures are seen in PCFs. In fact, it is possible to adjust elements like the number of propagating modes, attenuation, dispersion, and birefringence by changing the geometric parameters of the micro-structured coating. Traditional optical fibres feature a core and cladding-based construction that follows total internal reflection, however in PCF, the multicore structure follows improvised total internal reflection based on the photonic band-gap [10].

1.4 PCF BASED SPR SENSORS:

A simple, very sensitive photonic crystal fibre (PCF) temperature sensor is created using the surface plasmon resonance (SPR) theory. Two layers of square-shaped holes make up the majority of the sensor's covering. The essential process that allows the sensors with implanted PCF to function relies heavily on the transient field. An electromagnetic wave propagates further after striking a film-based core formed of plasmonic material until it reaches the cladding zone. The primary mechanism governing how sensors with implanted PCF function is dependent upon the transient field. The electromagnetic wave strikes the film-based core made of plasmonic material, and further propagation carries it to the region of cladding. The metal surface and the field interact electrons as it reaches the cladding region, causing oscillations at the surface. When light experiences complete internal reflection at the affiliate of two materials with various refractive indices, free electrons on the metal surface create coherent oscillations that culminate in the generation of plasmon

waves on the surface. The phenomenon of wavelength resonance between the incident wave and the transmitted or produced wave allows for narrowband resonance peaks and low propagation losses for incident light. For the net effective mode index, additional comparisons between the core mode and surface plasmon polarisation modes are made. The metals used to coat the cladding surface to improve the sensor occasionally oxidise during the process, which has a detrimental effect on the sensor's function. This can be avoided by using stable metals. Gold is the most widely used plasmonic material in this because it is stable and doesn't oxidise during sensing. The PCF-SPR sensor combines PCF and SPR technologies and has a flexible structural design with high sensing sensitivity. The cladding surface is covered with a layer of metal to improve the interactivity between the incident transient field and the unbounded electrons of the surface be able to increase the susceptibility of PCF-based surface plasmonic resonance sensors. For this, plasmonic materials are typically employed to create the metal films that are used [11]. In contrast, silver produces accurate findings and has a narrow resonance peak, but its oxidation has a negative effect on the sensor's function. Silver is frequently covered in a thin bimetallic coating to address the flaw. Due to its robust, stable characteristics and hexagonal form, which inhibits oxidation, graphene is typically utilised for this [9].

1.5 OBJECTIVE OF THE STUDY:

This study's objectives are to construct the SPR PCF sensor design using COMSOL Multi physics, examine the simulation's findings, and compare the sensor's sensitivity for the core and SPP modes as well as for a number of other parameters.

The simulation examines how the net effective mode index is affected by the wavelength, core radius, and substance of the incident light.

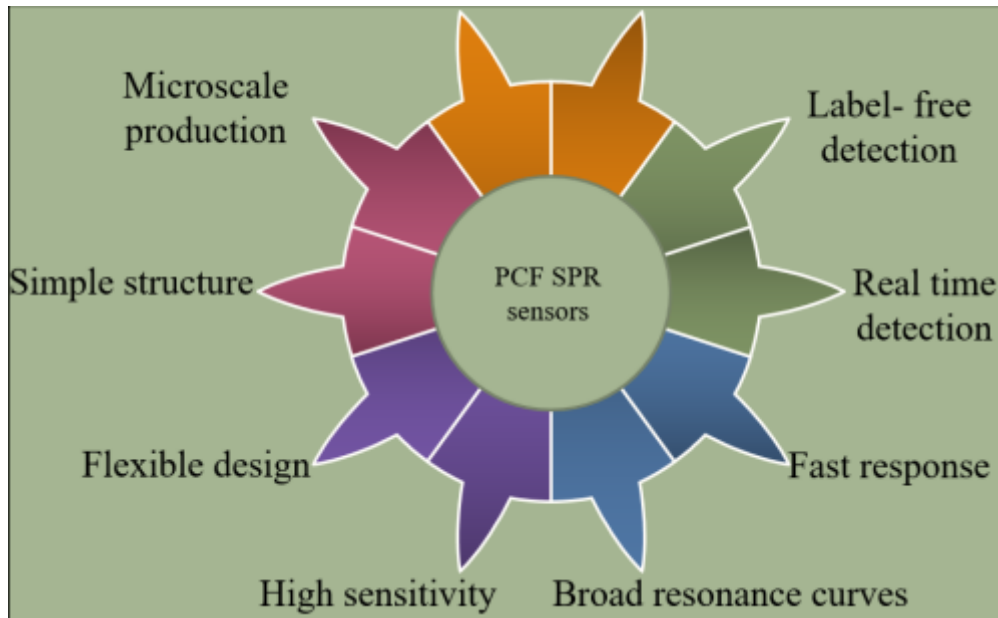


Figure 1.5: Advantages of PCF SPR sensors

CHAPTER 2

METHODOLOGY

2.1 NUMERICAL MODEL:

Figure shows the initial creation of the sensor's basic schematic. The schematic design displays the material option for the sensor. For resonance-induced electron conduction in the presence of incoming light, different plasmonic materials have been developed. Fused silica (SiO_2), the second material utilised, serves as a substrate and is put outside the air pores. Binding of the mobile molecules with the analyte in the analyte to the immobile molecules on the thin layer caused a change in the thin object's refractive index plasmonic material film. Also the outer layer contains SiO_2 , which acts as a shield between the analyte and the incoming light. The thin plasmonic material film's refractive index changes when light of a certain wavelength strikes the sensor's surface traversing the analyte, and into the SiO_2 where the molecules become mobilised and affixed to the stationary molecules of our plasmonic material silver. Version 5.6 of COMSOL Multiphysics employs the capabilities of the FEM. The forms that are seen in figure were created by the software. Air holes of varied diameters were used to sculpt the cladding in the model.

Diameters of the air holes are d_1 , d_2 , and d_3 , with values of 400 nm, 0.8 μm , and 1.6 μm correspondingly, have been taken as the parameters. The analyte's thickness is taken to be 2 μm , the plasmonic material's thickness layer to be 40 nm, and the incident wavelength to be 0.6 μm . The analyte's refractive index is equal to 1.38.

The DL model has been utilised to figure out the silver's dielectric constant. The Sellmeier equation can be used to determine SiO₂'s refractive index [12], [13]

$$n^2(\lambda) = 1 + \frac{B_1\lambda^2}{\lambda - C_1} + \frac{B_2\lambda^2}{\lambda - C_2} + \frac{B_3\lambda^2}{\lambda - C_3} \quad (1)$$

Where the wavelength (λ) in μm , B_1 , B_2 , B_3 , and C_1 , C_2 , C_3 are the Sellmeier coefficients, and the first term represents the square of silica's refractive index.

Now, we can use the following equation to determine the confinement loss of the sensor:

$$\alpha_{loss} = 8.856 \times \frac{2\pi}{\lambda} \times \text{Im}(n_{eff}) \times 10^4 \text{ dB/cm} \quad (2)$$

Where the imaginary component of the net effective refractive index is $\text{Im}(n_{eff})$ and is the wavelength (λ) in μm .

There are two ways to measure a sensor's sensitivity: amplitude sensitivity and wavelength sensitivity. Use the following equation to get the wavelength sensitivity:

$$S_W(\lambda) = \frac{\Delta\lambda_{peak}}{\Delta n_a} \quad (3)$$

Where, $\Delta\lambda$ denotes the shift in resonant peaks caused by the shift in refractive indices, or Δn_a

The following formula is employed to determine the amplitude sensitivity.

$$S_a(\lambda) = -\frac{1}{a(\lambda, n_a)} \frac{\delta a(\lambda, n_a)}{\delta n_a} \quad (4)$$

The smallest variation in the measurement of the desired amount is referred to as sensor resolution. Thus, it is crucial to calculate sensor resolution.

The following equation can be used to determine the sensor resolution.

$$R = \frac{\Delta n_a \Delta \lambda_{min}}{\Delta \lambda_{peak}} \quad (5)$$

Here, the following equation is used to compute the sensor resolution. The variations in the minimal wavelength resolution, and the refractive index, and the peak shift of the resonant wavelengths are denoted, respectively, by the letters Δn_a , $\Delta \lambda_{min}$, and $\Delta \lambda_{peak}$.

2.2 SIMULATION MODEL:

In COMSOL Multi-physics, the Wave optics module is chosen in order to move on with the model's operation, and the time-dependent equation package is chosen under the Study section. The following variables are introduced for resolving the DL model equations in order to specify the model's geometry. While the operational wavelength, which is first set at 0.6 μm and is adjusted up to 2 μm to see the net effective mode index, is a variable and initially set at 0.6 μm , the other necessary parameters for the model are fixed and remain constant throughout the whole analysis of the sensor. Additionally, a study model of the frequency domain that analyses the model along with its frequency at various domains scales the model for the electromagnetic waves interface. The common wavelength taken from the physics interface is used in conjunction with the polynomial coordinate stretching type.

CHAPTER 3

DESIGN AND MODELLING

3.1 STRUCTURAL DESIGN FOR THE THIN FILM BASED PCF SENSOR:

The basic schematic that was developed for the sensor as a starting point is shown in Figure 3.1. The schematic design displays the material option for the sensor. The sensor's material selection is shown in the schematic design. Following the resonance condition, the plasmonic component is composed of silver for the electrons to conduct through in the presence of the incoming light. Fused silica (SiO_2), the second material employed, is poured into the space outside the air holes to act as a substrate. For the electrons' conductivity when there is the incoming light after the resonance state, many plasmonic materials have been used. Fused silica (SiO_2), the second material employed, serves as a substrate and is deposited in the exterior area. The thin plasmonic material film's refractive index changed resulting from the analyte's utilize to bind the mobile molecules in the analyte to the immobile molecules within the thin layer. The outer layer also contains SiO_2 , which acts as a shield between the analyte and the incoming light. The fundamental concept is to illuminate the sensor's surface with light of a specific wavelength, which passes from the analyte to the SiO_2 , where the molecules become mobilised and attached to the silver molecules that are stationary in our plasmonic material, changing the thin sheet of plasmonic material's refractive index. It is poured in between the air holes. The employment of the analyte to bind the mobile molecules in the

analyte to the immobile molecules on the thin layer caused a change in the thin plasmonic material film's refractive index.

SiO₂ is also present in the outer layer to serve as a bridge between an instance and the light being incident. The main idea is to illuminate the surface of the sensor with light of a particular wavelength. The SiO₂ molecules are mobilised and bonded to the immobile silver molecules in our plasmonic material, changing the refractive index of the thin plasmonic material film as the light then passes through the analyte to the SiO₂ layer.

Here, the COMSOL Multi-physics software version 5.6 has been used to apply the FEM. The programme has been used to build the shapes that are seen in the figure. Air holes with various diameters have been used in the model to shape the cladding.

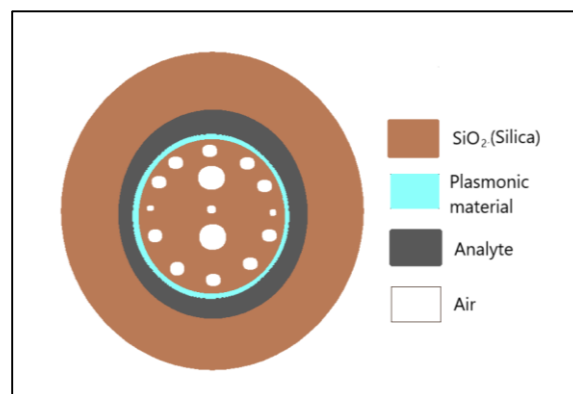


Figure 3.1: The desired sensor model is depicted schematically.

The analyte-filled structure has air holes inside of it, as seen in the picture, and the sizes were chosen to make the construction efficient and small.

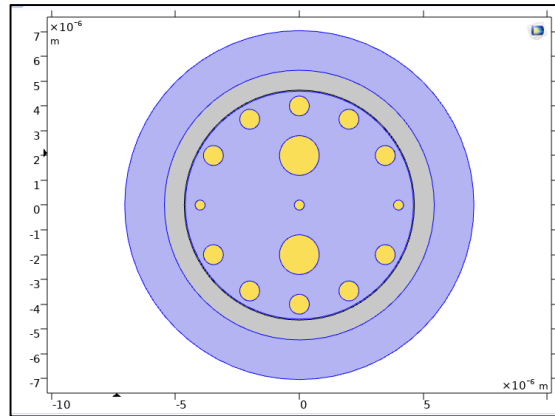


Figure 3.2: Model structure in COMSOL

d_1 , d_2 , and d_3 are the air hole diameters, measuring 400 nm, 0.8 μm , and 1.6 μm are the parameters that have been taken. The analyte's thickness, t_a , is 2 μm , the plasmonic material layer's thickness, t_g , is taken to be 40 nm, and the incidence wavelength, λ , is 0.6 μm . The analyte's refractive index, n_a , is equal to 1.38.

CHAPTER 4

RESULT AND DISCUSSION

When the model's structure has been correctly designed, the confinement losses and sensitivities for each material are estimated, and they are then displayed versus wavelength for various refractive indices.

An examination of the net effective mode refractive index fluctuation for a dual core PCF sensor based on silver thin film:

Figure 4.1 depicts the sensor's core and SPP modes (a) and (b). The magnetic fields are observed propagating first highlighted from left to right section of the core mode, and in the second highlighted area, from right to left.

Lines of the magnetic field in the SPP mode run from downward to upward. The representation of the respective effective refractive indices at the wavelength by both of these modes has been established value of $=6.857E-7m$.

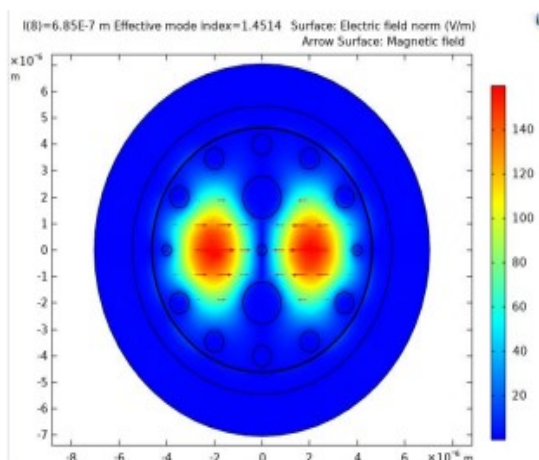


Fig.4.1. (a) Core mode $n_{eff}=1.4514$

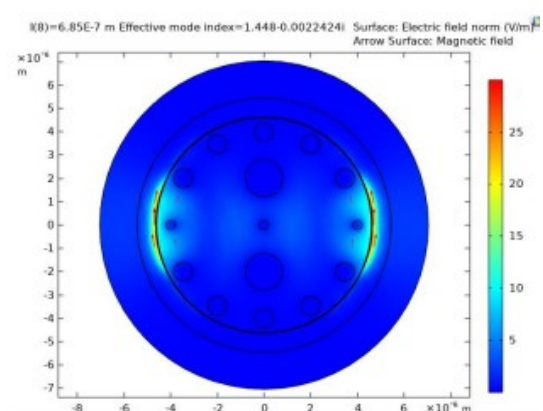


Fig.4.1. (b) SPP mode $n_{eff} = 1.448-0.0022424i$

By varying the refractive index values, multiple arrangements of the created design model can be viewed. For the many modes that can be accomplished, we have estimated the various values of net effective refractive indices.

4.1 PHASE MATCHING:

While they are present at the edge of the plasmonic material in the SPP mode, the model's structure for the sensor's core mode includes magnetic field lines in the x and y dimensions. Equation (2) is used to determine the confinement loss of the sensor, and a graph plotting the wavelength against the x- and y-polarizations is then created. The phase matching wavelength peak value is then recorded, and the phase matching curve (figures 4.2 and 4.3) is obtained.

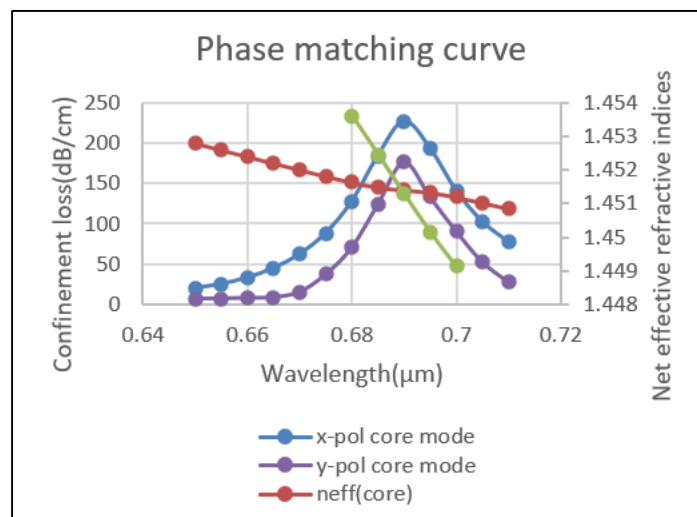


Figure 4.2: Core and SPP mode phase matching curve for gold nanofilm

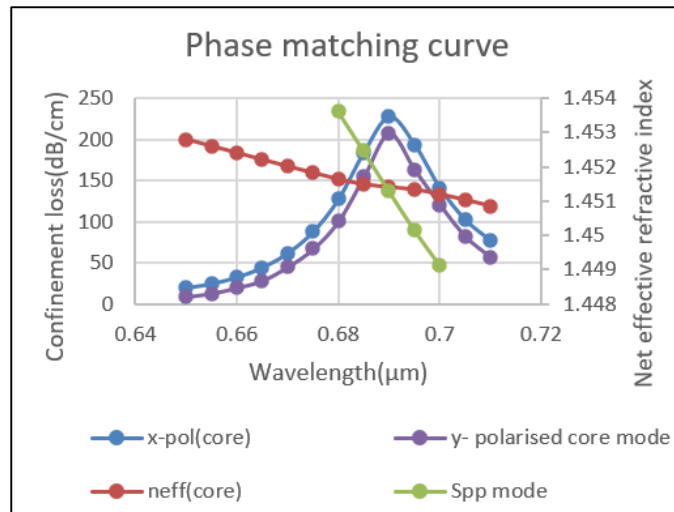


Figure 4.3: Core and SPP mode phase matching curve for silver nanofilm

With wavelengths ranging from 0.5-0.65 μm , the materials, confinement losses, and refractive indices are adjusted for lower ranges of 1.25-1.30. The following curves display the confinement loss curves that were used to determine the wavelength sensitivity. The thickness of gold nanofilm at 40nm reveals the confinement loss curve shown below.

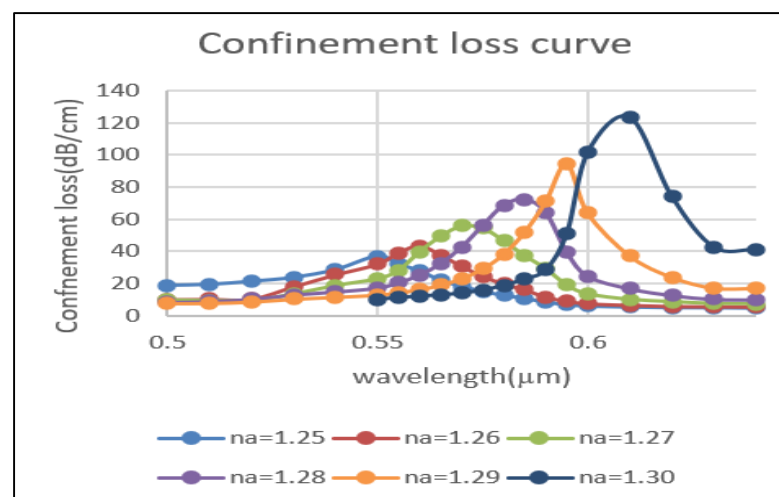


Figure 4.4: Curve of confinement loss for gold nanofilm ($n_a=1.25-1.30$)

For the silver nanofilm at a thickness of 40nm, the confinement loss curve is shown in the following. (Figure 4.5)

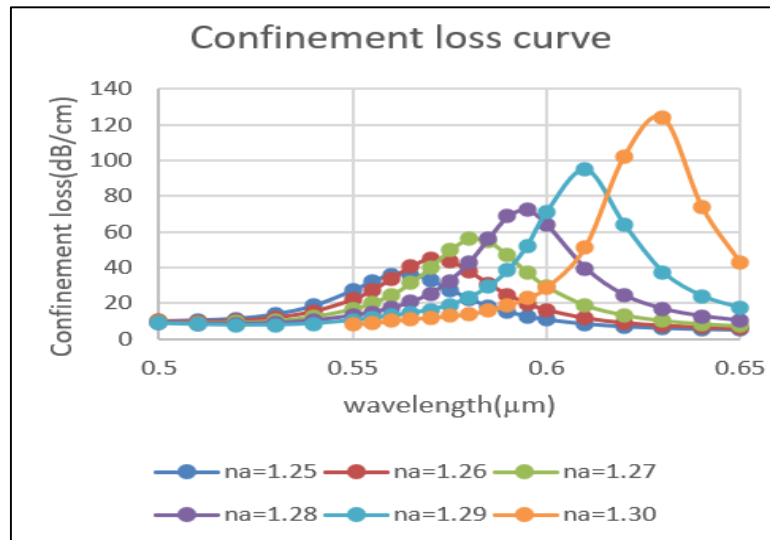


Figure 4.5: Curve of confinement loss for silver nanofilm ($n_a=1.25-1.30$)

Figures 4.6, 4.7 and 4.8 illustrate, respectively, the confinement loss curves for nanofilms of aluminium, copper, and gold-tin alloy with a thickness of 40 nm. Contrary to the gold tin alloy curve, which has a more rounded confinement loss peak, aluminium and copper have sharper peaks.

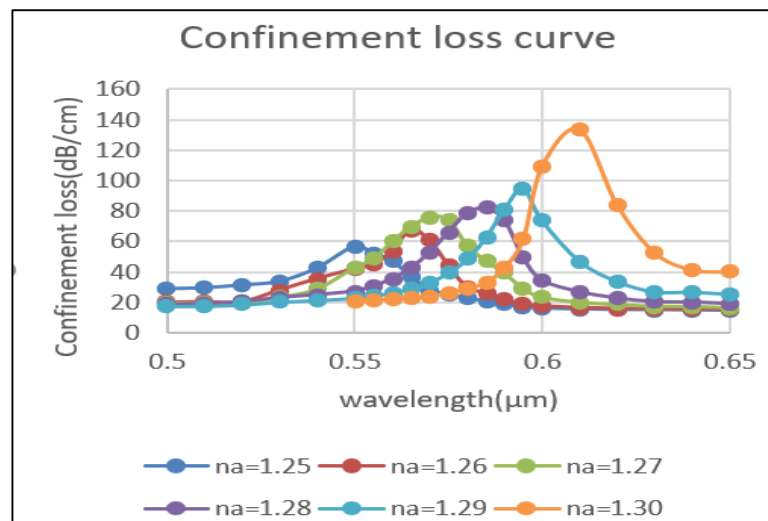


Figure 4.6: Curve of confinement loss for aluminium nanofilm ($n_a=1.25-1.30$)

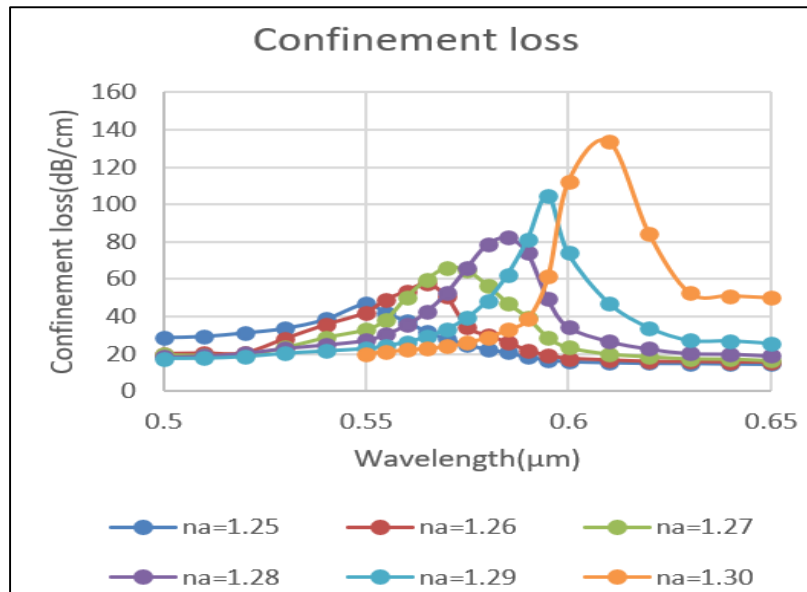


Figure 4.7 Curve of confinement loss for copper nanofilm ($n_a=1.25-1.30$)

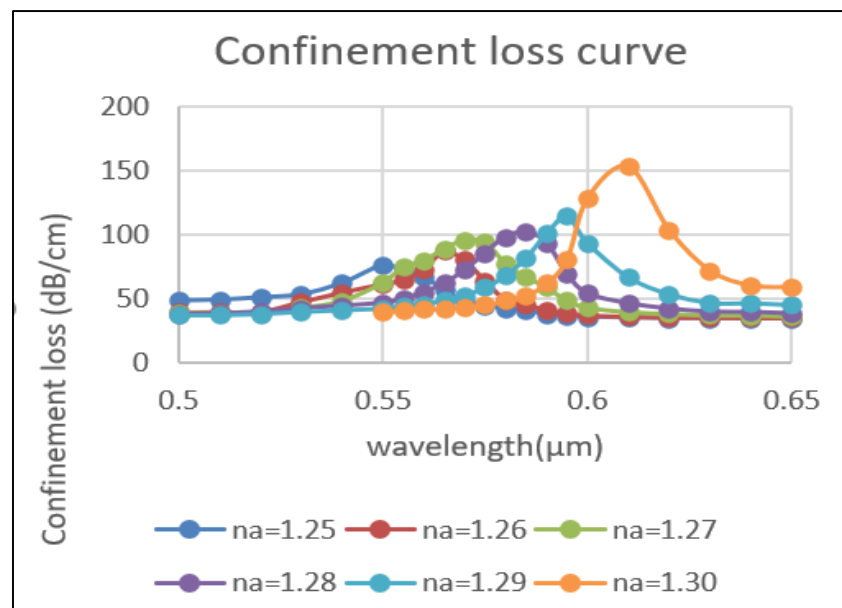


Figure. 4.8 Curve of confinement loss for for gold-tin nanofilm ($n_a=1.25-1.30$)

4.2 CALCULATION OF WAVELENGTH SENSITIVITIES:

In the event that the refractive indices alter from $n_a=1.25$ to $n_a=1.30$, Equation (3) can be used to calculate the wavelength sensitivities for gold, silver, and aluminium nanofilms.

The table for observed (R2-R1) and peak values .

Plasmonic material	Δn_a (R2-R1)	$\Delta \lambda_{\text{peak}}$	nmRIU ⁻¹
Gold	0.05	91.538	1830.76
Silver	0.05	89.95	1799.00
Aluminium	0.05	86.61	1732.20
Copper	0.05	82.60	1652.00
Gold-tin	0.05	76.61	1532.2

Table 1. Wavelength sensitivities for different materials

As a result, all three materials had wavelength sensitivities of the same order of 10^3 nmRIU⁻¹

4.3 CALCULATION OF AMPLITUDE SENSITIVITIES:

For the three materials, we have displayed the amplitude sensitivities versus wavelength. using equation (4) to determine each material's amplitude sensitivities for the refractive index range of 1.25 to 1.30. The estimated amplitude shows variance for various wavelengths and refractive indices. The amplitude sensitivity is seen to increase gradually as the wavelength is increased before dropping abruptly. Meanwhile, bigger peaks are seen for the larger refractive indices than for the lower refractive indices.

Figures 4.9 to 5.13 illustrate how, for each plasmonic material, amplitude sensitivity varies in relation to wavelength for various refractive indices.

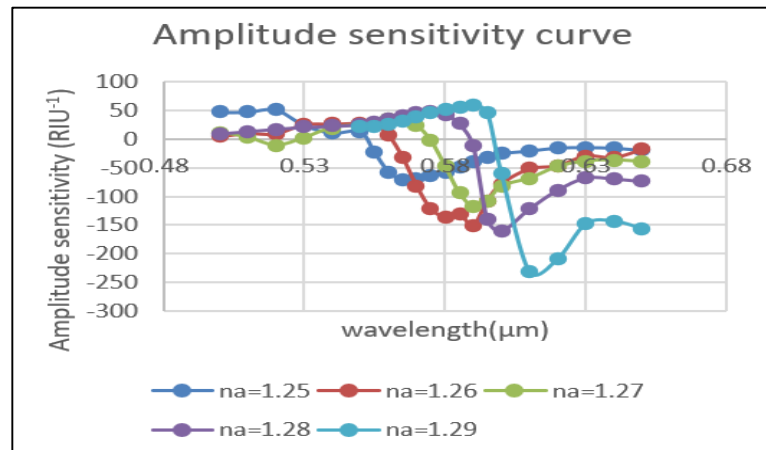


Figure 4.9. Amplitude sensitivity curve for gold nanofilm $n_a=1.25-1.30$

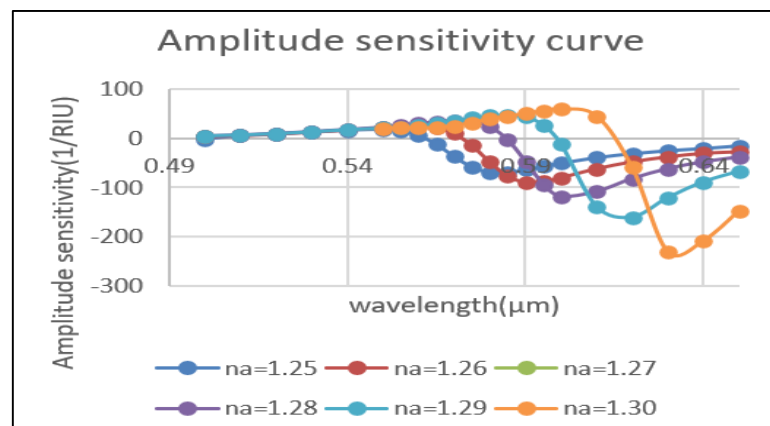


Figure 4.10: Amplitude sensitivity curve for silver nanofilm $n_a=1.25-1.30$

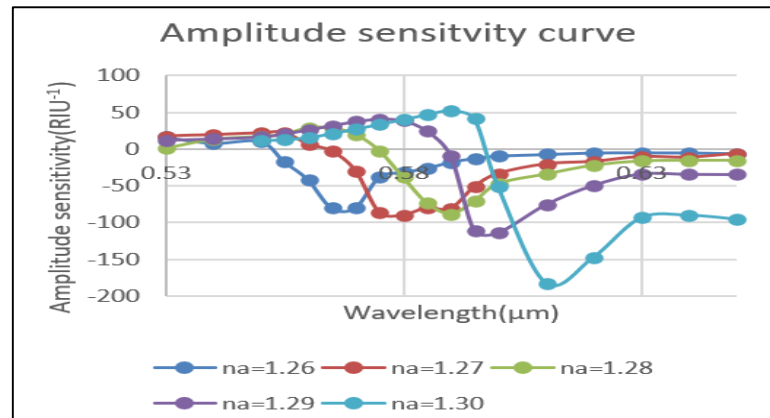


Figure 4.11. Amplitude sensitivity curve for aluminium nanofilm $n_a=1.25-1.30$

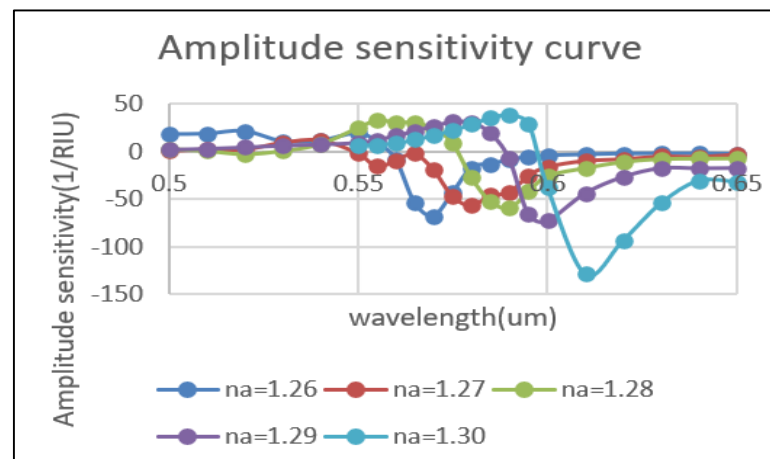


Figure 4.12: Amplitude sensitivity curve for Copper nanofilm $n_a=1.25-1.30$

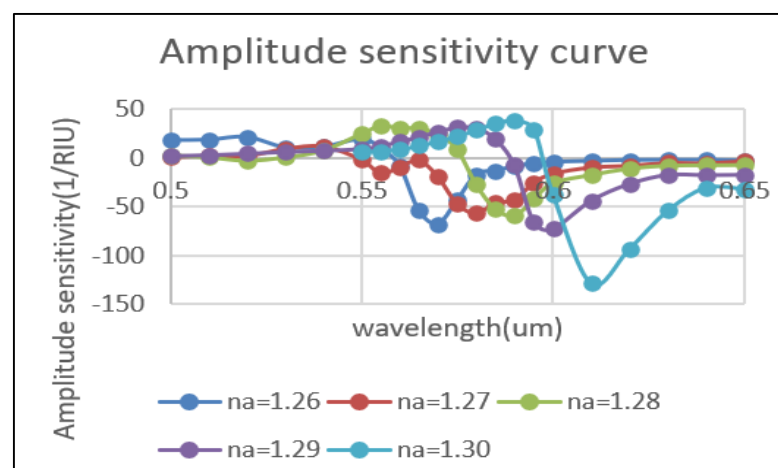


Figure 4.13: Amplitude sensitivity curve for gold-tin alloy nanofilm $n_a=1.25-1.30$

The so obtained amplitude sensitivities range for each of the plasmonic materials is noted and compared. It is demonstrated that gold and silver are the plasmonic materials that yield the best results after comparing the amplitude and wavelength sensitivity. These materials are therefore commonly employed. In order creating the sensor more accessible and suitable having favourable outcomes, aluminium nano film is suggested.

CHAPTER 5

COMPARISON OF DIFFERENT PHOTONIC CRYSTAL FIBER:

These PCFs come in two varieties: solid core and a hollow core. This study proposes a survey for various PCF shapes by using different background materials. Comparing the sensitivity and confinement loss using this PCF of various shapes with various background materials [14]

The periodic arrangement of the dielectric materials that make up the Photonic Crystal modifies the propagation characteristics [15]–[18]. Numerous applications, including bio-sensing, biomedical, chemical sensing, and gas sensing, use PCF. Different PCFs have been utilised for chemical sensing in recent years [19].

5.1 SENSIBLE PHOTONIC CRYSTALS:

The sensible photonic crystal is built using a modified hexagonal structure to assess the sensitivity of substances with lower refractive indices, such as ethanol, water, and benzene. It measures a number of variables, including non-linearity, beam divergence, spot size, and confinement loss. With this method, it is possible to independently change the hole's shape, size, and distance. The air hole can also rotate. Ethyl alcohol, benzene, and water are placed into the air holes in order to analyse various liquids. Software called COMSOL Multi-physics was used in this case. In order to calculate the confinement loss, a fictitious portion of the effective index n_{eff} term is employed. Here, as the outer ring diameter value rises, the sensitivity rises as well. This technique coats the background

with silica, and the outside rings are known as air gaps. The fibre structure's middle contained the core fault.

5.2 RECTANGULAR HOLLOW CORE PHOTONIC CRYSTALS:

The analyser was put inside a hollow-core PCF (HC-PCF) with a rectangular shape. The core region has air holes, and the cladding region has circular holes. By satisfying the boundary conditions, FEM is used to implement the light directing characteristics. It has greater sensitivity. It has low confinement loss. [20] .

5.3 OCTAGONAL PHOTONIC CRYSTALS:

In this research, an octagonal photonic crystal fibre (O-PCF) utilised to feel the liquid had a micro-structured centre and an outer shell. By using FEM, the propagation properties were examined. Analysis of confinement loss and sensitivity was done here. Sensitivity of 46.3% was achieved. It has low confinement loss. [21]

5.4 MULTIPLE SENSING RING PHOTONIC CRYSTAL:

This technique allowed for the chemical's detection. The backdrop substance was silicon in the FEM analysis. To interact with the components, the light moves within the ring construction. Based on each material's RI term, the relationship between light and that substance. Sensitivity of 95.40% and 93.13% was achieved. [22]. Depending on the appropriate choice of air ratios, pitch, air hole diameter, and operating wavelength, the confinement loss can be decreased. According to the findings, three rings have a lower RI than four rings.

5.5 ORTHOGONAL PHOTONIC CRYSTAL:

To detect ethanol, an orthogonal photonic crystal was suggested to detect liquid, elliptical holes and a hexagonal lattice are present. Background material utilised was Pure Silica

Gel. It has good sensitivity [23]. The core was filled with the detecting liquid, ethanol. FEM was used to mathematically analyse confinement loss and sensitivity. It was discovered that for the wavelength of 1.33 μm , reduced confinement loss and increased sensitivity are produced by elliptical holes in the middle region.

5.6 CIRCULAR PATTERN CRYSTAL FIBER:

Sensitivity, confinement loss, non-linearity, and effective area were calculated in this case. [24].

The light leaking that caused the confinement loss. There were five rings in the three circles in the core and cladding. The centre of the device was filled with several liquids, including glycerol, ethanol, and toluene. FEM was used to analyse the sensitivity and confinement losses. The confinement loss was brought on by the light leak. The cladding had five rings and the core had three rings. Glycerol, ethanol, and toluene were among the liquids present in the device's centre. The analysis of the sensitivity and confinement losses was done using FEM.

5.7 CONCLUSION:

Several structures, including hexagonal, rectangular hollow core, octagonal, and circular-pattern photonic structures are compared. Discovering the sensitivity and confinement loss is the key goal. Applications for this PCF include bio-sensing, biomedical, chemical sensing, and gas sensing.

CHAPTER 6

SUMMARY

In the present study, we have constructed an SPR-based PCF sensor with fixed parameters such as thickness, area, and distance as well as changeable elements such as wavelength, refractive index, and plasmonic material. Gold, silver, aluminium, copper, and gold-tin alloys are suitable for various plasmonic materials. We have determined the wavelength sensitivity by plotting the confinement loss curves. Gold has the highest wavelength sensitivity, or 1830.76 nm/RIU, followed by silver with a sensitivity of 1799 nm/RIU, and aluminium with a sensitivity of 1732 nm/RIU. The wavelength sensitivity for copper is 1652 nm/RIU, while for the gold-and-silver alloy, it is 1532.2 nm/RIU. When the materials' amplitude sensitivities are plotted against a change in wavelength, silver nanofilm exhibits the finest curve. The sensor's average resolution is estimated to be of the order of 10^{-5} . So long as the right set of characteristics are specified, any material can be used for efficient sensing. SPR-based biosensors have numerous applications, including environmental monitoring, medical diagnostics, food safety to security, and food analyte detection.

CHAPTER 7

FUTURE WORK

The number of human diseases has been gradually rising for many years. We need to develop sensing technology that is both user and sensor-friendly. The huge list of biomarkers linked to various cancers and harmful illnesses could be useful for a robotic biosensor technology, but it confronts a number of challenges. The focus is on obtaining robust, cost-effective platforms for multiple analyte detection biosensors as the instrumentation difficulty persists. Improving the high-frequency performance of waveguide- and fiber-based SPR for a variety of applications is a different issue. The fabrication of a practical sensor, analysis with regard to a variety of refractive indices, implantation in devices for sensing in practical applications, and greater variety of chemical and biological applications for analyte detection are the future potential of SPR PCF sensors. The replacement of the existing particular equipment is the goal in the future. To be used are the benefits of SPR-based PCF sensors, such as label-free detection, low cost, and effective applications. Due to their complex designs, the prism-based SPR sensors must be updated and implanted in the practical devices. The materials' inner and outer coating-related structures have been documented thus far. The D-shaped sensors are greatly developed for the practical applications due to the factor of sensitivity.

REFERENCES


- [1] S. Mittal, T. Sharma, and M. Tiwari, "Surface plasmon resonance based photonic crystal fiber biosensors: A review," *Mater. Today Proc.*, vol. 43, pp. 3071–3074, 2021, doi: 10.1016/j.matpr.2021.01.405.
- [2] J. Homola, "Surface Plasmon Resonance Sensors for Detection of Chemical and Biological Species," *Chem. Rev.*, vol. 108, no. 2, pp. 462–493, Feb. 2008, doi: 10.1021/cr068107d.
- [3] Md. R. Hasan, S. Akter, K. Ahmed, and D. Abbott, "Plasmonic Refractive Index Sensor Employing Niobium Nanofilm on Photonic Crystal Fiber," *IEEE Photonics Technol. Lett.*, vol. 30, no. 4, pp. 315–318, Feb. 2018, doi: 10.1109/LPT.2017.2786475.
- [4] E. Haque, S. Mahmuda, Md. A. Hossain, N. H. Hai, Y. Namihira, and F. Ahmed, "Highly Sensitive Dual-Core PCF Based Plasmonic Refractive Index Sensor for Low Refractive Index Detection," *IEEE Photonics J.*, vol. 11, no. 5, pp. 1–9, Oct. 2019, doi: 10.1109/JPHOT.2019.2931713.
- [5] T. A. Roni, R. Hassan, and M. Faisal, "Dual-Side Polished SPR Biosensor with Wide Sensing Range," in *2020 11th International Conference on Electrical and Computer Engineering (ICECE)*, Dhaka, Bangladesh: IEEE, Dec. 2020, pp. 487–490. doi: 10.1109/ICECE51571.2020.9393102.
- [6] A. A. Rifat, R. Ahmed, G. A. Mahdiraji, and F. R. M. Adikan, "Highly Sensitive D-Shaped Photonic Crystal Fiber-Based Plasmonic Biosensor in Visible to Near-IR," *IEEE Sens. J.*, vol. 17, no. 9, pp. 2776–2783, May 2017, doi: 10.1109/JSEN.2017.2677473.
- [7] J. Lu, Y. Li, Y. Han, Y. Liu, and J. Gao, "D-shaped photonic crystal fiber plasmonic refractive index sensor based on gold grating," *Appl. Opt.*, vol. 57, no. 19, p. 5268, Jul. 2018, doi: 10.1364/AO.57.005268.
- [8] E. Kretschmann and H. Raether, "Notizen: Radiative Decay of Non Radiative Surface Plasmons Excited by Light," *Z. Für Naturforschung A*, vol. 23, no. 12, pp. 2135–2136, Dec. 1968, doi: 10.1515/zna-1968-1247.
- [9] S. Zhang, J. Li, S. Li, Q. Liu, J. Wu, and Y. Guo, "Surface plasmon resonance sensor based on D-shaped photonic crystal fiber with two micro-openings," *J. Phys. Appl. Phys.*, vol. 51, no. 30, p. 305104, Aug. 2018, doi: 10.1088/1361-6463/aace72.
- [10] B. Lee, S. Roh, and J. Park, "Current status of micro- and nano-structured optical fiber sensors," *Opt. Fiber Technol.*, vol. 15, no. 3, pp. 209–221, Jun. 2009, doi: 10.1016/j.yofte.2009.02.006.
- [11] V. Kaur and S. Singh, "Design of D-Shaped PCF-SPR sensor with dual coating of ITO and ZnO conducting metal oxide," *Optik*, vol. 220, p. 165135, Oct. 2020, doi: 10.1016/j.ijleo.2020.165135.

- [12] A. Hassani and M. Skorobogatiy, "Design criteria for microstructured-optical-fiber-based surface-plasmon-resonance sensors," *J. Opt. Soc. Am. B*, vol. 24, no. 6, p. 1423, Jun. 2007, doi: 10.1364/JOSAB.24.001423.
- [13] C. Liu *et al.*, "Symmetrical dual D-shape photonic crystal fibers for surface plasmon resonance sensing," *Opt. Express*, vol. 26, no. 7, p. 9039, Apr. 2018, doi: 10.1364/OE.26.009039.
- [14] S. Mohamed Nizar, S. Rafi Ahamed, E. Priyanka, R. Jayasri, and B. Kesavaraman, "Comparison of Different Photonic Crystal Fiber Structure: A Review," *J. Phys. Conf. Ser.*, vol. 1717, no. 1, p. 012048, Jan. 2021, doi: 10.1088/1742-6596/1717/1/012048.
- [15] T. A. Birks, J. C. Knight, and P. St. J. Russell, "Endlessly single-mode photonic crystal fiber," *Opt. Lett.*, vol. 22, no. 13, p. 961, Jul. 1997, doi: 10.1364/OL.22.000961.
- [16] N. Luan, R. Wang, W. Lv, Y. Lu, and J. Yao, "Surface Plasmon Resonance Temperature Sensor Based on Photonic Crystal Fibers Randomly Filled with Silver Nanowires," *Sensors*, vol. 14, no. 9, pp. 16035–16045, Aug. 2014, doi: 10.3390/s140916035.
- [17] H. Ebendorff-Heidepriem *et al.*, "Bismuth glass holey fibers with high nonlinearity," *Opt. Express*, vol. 12, no. 21, p. 5082, 2004, doi: 10.1364/OPEX.12.005082.
- [18] Md. F. H. Arif, K. Ahmed, S. Asaduzzaman, and Md. A. K. Azad, "Design and optimization of photonic crystal fiber for liquid sensing applications," *Photonic Sens.*, vol. 6, no. 3, pp. 279–288, Sep. 2016, doi: 10.1007/s13320-016-0323-y.
- [19] H. Ademgil, "Highly sensitive octagonal photonic crystal fiber based sensor," *Optik*, vol. 125, no. 20, pp. 6274–6278, Oct. 2014, doi: 10.1016/j.ijleo.2014.08.018.
- [20] Md. M. Hasan, T. Pandey, and Md. A. Habib, "Highly sensitive hollow-core fiber for spectroscopic sensing applications," *Sens. Bio-Sens. Res.*, vol. 34, p. 100456, Dec. 2021, doi: 10.1016/j.sbsr.2021.100456.
- [21] B. K. Paul, K. Ahmed, S. Asaduzzaman, and Md. S. Islam, "Folded cladding porous shaped photonic crystal fiber with high sensitivity in optical sensing applications: Design and analysis," *Sens. Bio-Sens. Res.*, vol. 12, pp. 36–42, Feb. 2017, doi: 10.1016/j.sbsr.2016.11.005.
- [22] V. Kaur and S. Singh, "Extremely sensitive multiple sensing ring PCF sensor for lower indexed chemical detection," *Sens. Bio-Sens. Res.*, vol. 15, pp. 12–16, Sep. 2017, doi: 10.1016/j.sbsr.2017.05.001.
- [23] A. K. Ghunawat, S. Sharma, S. Sahu, and G. Singh, "Highly Sensitive Octagonal Photonic Crystal Fiber for Ethanol Detection," in *Optical and Wireless Technologies*, V. Janyani, G. Singh, M. Tiwari, and A. d'Alessandro, Eds., in Lecture Notes in Electrical Engineering, vol. 546. Singapore: Springer Singapore, 2020, pp. 457–466. doi: 10.1007/978-981-13-6159-3_48.

- [24] R. Senthil, A. Soni, K. Bir, R. Senthil, and P. Krishnan, "Circular-Pattern Photonic Crystal Fiber for Different Liquids with High Effective Area and Sensitivity," *Plasmonics*, vol. 14, no. 6, pp. 1783–1787, Dec. 2019, doi: 10.1007/s11468-019-00977-y.
- [25] N. Sabri, S. A. Aljunid, M. S. Salim, R. B. Ahmad, and R. Kamaruddin, "Toward Optical Sensors: Review and Applications," *J. Phys. Conf. Ser.*, vol. 423, p. 012064, Apr. 2013, doi: 10.1088/1742-6596/423/1/012064.

APPENDICES

APPENDIX 1: PLAGIARISM REPORT


Similarity Report ID: oid:27535:36342876

● 9% Overall Similarity

Top sources found in the following databases:

- 2% Internet database
- 8% Publications database
- Crossref database
- Crossref Posted Content database
- 2% Submitted Works database

TOP SOURCES

The sources with the highest number of matches within the submission. Overlapping sources will not be displayed.

1	Deepak Kumar, Madhur Khurana, Mukta Sharma, Vinod Singh. "Analog... <small>Crossref</small>	4%
2	S. Mohamed Nizar, S. Rafi Ahamed, E. Priyanka, R. Jayasri, B. Kesavara... <small>Crossref</small>	<1%
3	Deepak Kumar, Mukta Sharma, Vinod Singh. "Surface Plasmon resona... <small>Crossref</small>	<1%
4	Abdullah Mohammad Tanvirul Hoque, Kusay Faisal Al-tabatabaie, Md. ... <small>Crossref</small>	<1%
5	Emranul Haque, Abdullah Al Noman, Md. Anwar Hossain, Nguyen Hoan... <small>Crossref</small>	<1%
6	opg.optica.org <small>Internet</small>	<1%
7	Maddala Rachana, Ipshitha Charles, Sandip Swarnakar, Sabbi Vamshi ... <small>Crossref</small>	<1%
8	Universiti Tunku Abdul Rahman on 2013-04-19 <small>Submitted works</small>	<1%

[Sources overview](#)

PAPER NAME
madhur plag report.pdf

WORD COUNT
5968 Words

CHARACTER COUNT
32237 Characters

PAGE COUNT
33 Pages

FILE SIZE
1.5MB

SUBMISSION DATE
May 28, 2023 3:00 PM GMT+5:30

REPORT DATE
May 28, 2023 3:01 PM GMT+5:30

- **9% Overall Similarity**
The combined total of all matches, including overlapping sources, for each database.
 - 2% Internet database
 - 8% Publications database
 - Crossref database
 - Crossref Posted Content database
 - 2% Submitted Works database
- **Excluded from Similarity Report**
 - Bibliographic material
 - Small Matches (Less than 8 words)

Summary

9	University of Aberdeen on 2018-08-13 Submitted works	<1%
10	osapublishing.org Internet	<1%
11	Mohammad Al Mahfuz, Md. Anwar Hossain, Emranul Haque, Nguyen H... Crossref	<1%
12	University of Southampton on 2014-05-19 Submitted works	<1%
13	link.springer.com Internet	<1%
14	researchgate.net Internet	<1%
15	Guangyao Wang, Shuguang Li, Guowen An, Xinyu Wang, Yunyan Zhao, ... Crossref	<1%
16	Kawsar Ahmed, Sayed Asaduzzaman, Faizul Huq Arif. "Numerical anal... Crossref	<1%
17	Sheikh Shahriar Hossain, Md Rejvi Kaysir, Md Jahirul Islam, Elora Nahl... Crossref	<1%
18	Universiti Brunel Darussalam on 2022-04-26 Submitted works	<1%
19	University of Nottingham on 2022-11-14 Submitted works	<1%
20	lib.buet.ac.bd:8080 Internet	<1%

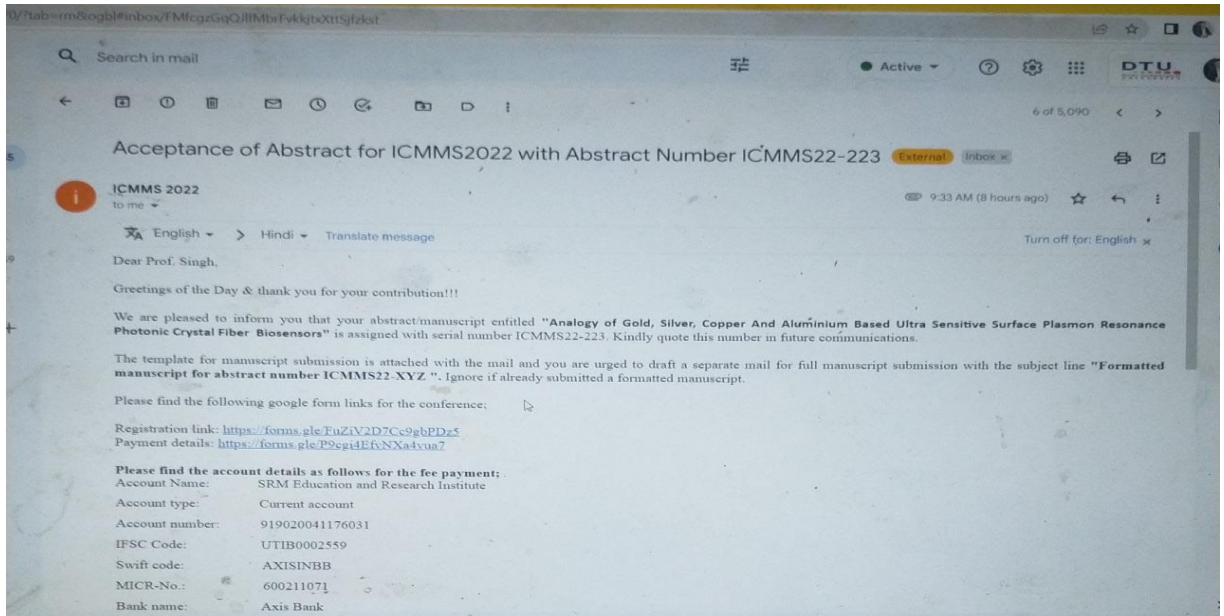
Sources overview

21	vdoc.pub Internet	<1%
22	xn--webeducation-dbb.com Internet	<1%

Sources overview



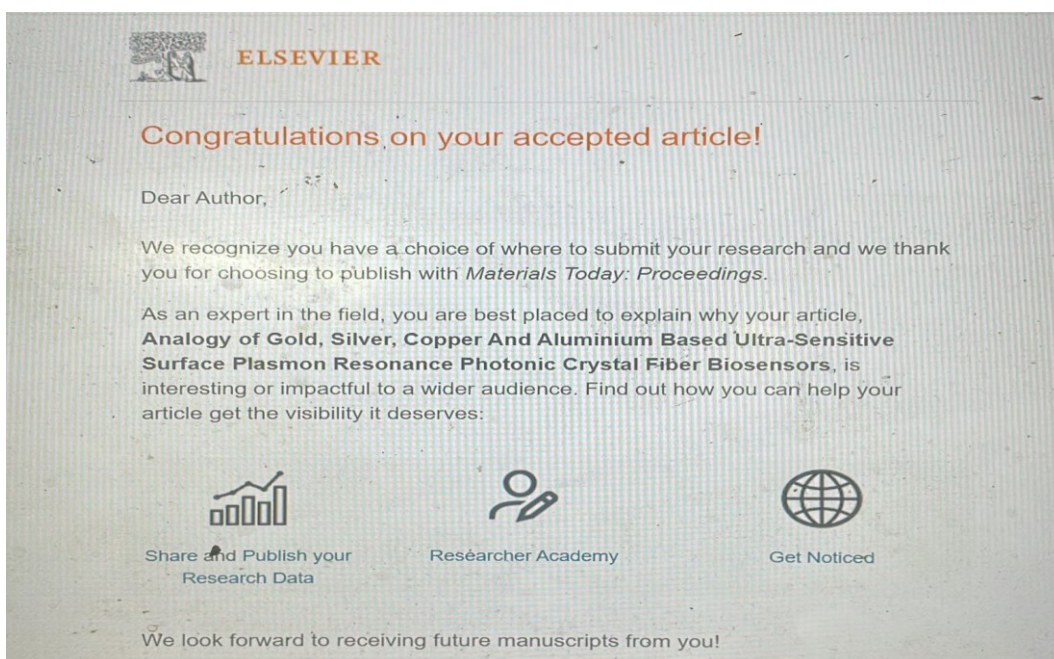
APENDIX 2: ABSTRACT ACCEPTANCE:



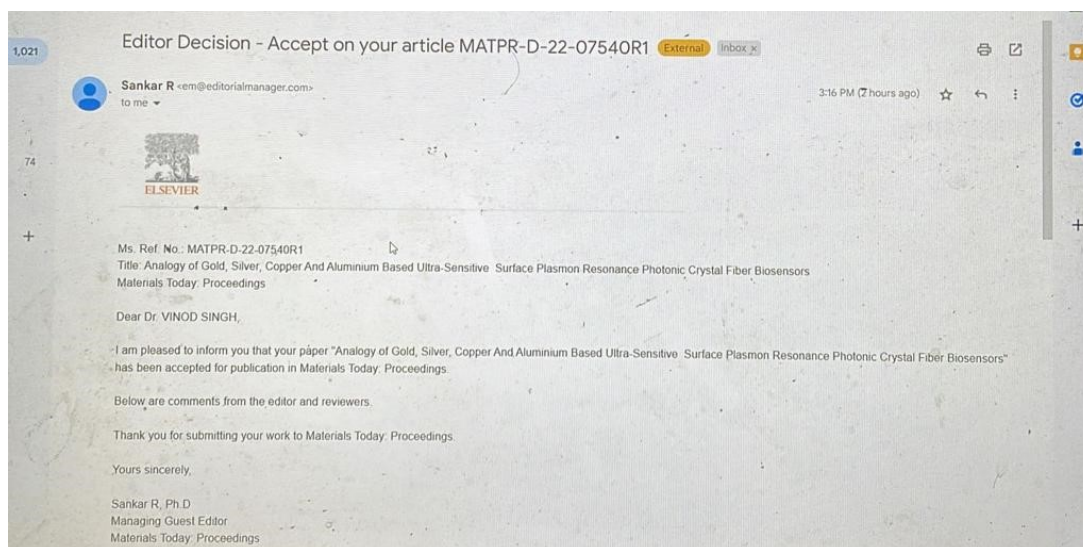
APPENDIX 3: CONFERENCE CERTIFICATE



APPENDIX 4: PROOF OF SCOPUS INDEX



APPENDIX 5: PAPER ACCEPTANCE



APPENDIX 6: RESEARCH PAPER

Materials Today: Proceedings xxx (xxxx) xxx



Contents lists available at ScienceDirect

Materials Today: Proceedings

journal homepage: www.elsevier.com/locate/matpr

Analogy of gold, silver, copper and aluminium based ultra-sensitive surface plasmon resonance photonic crystal fiber biosensors

Deepak Kumar¹, Madhur Khurana¹, Mukta Sharma¹, Vinod Singh^{1,*}

Department of Applied Physics, Delhi Technological University, Delhi 110042, India

ARTICLE INFO

Article history:
Available online xxxxx

Keywords:
Biosensors
Nanofilms
Plasmonic Crystal Fiber
Surface Plasmonic Resonance
Sensor modeling
Fiber optic sensors

ABSTRACT

In recent years, biosensors are being used for various medical and pharmaceutical purposes. For the formation of biosensors, one of the most commonly used phenomena is Surface Plasmon Resonance. Usually, biosensors are fabricated from optical fibers. However, when optical fibers are replaced with Photonic crystal fibers, the sensing properties are enhanced in a great way. These sensors are designed in such a way that a thin nanofilm of plasmonic metals like Gold, Silver, copper, aluminium, and plasmonic metal alloy gold-tin surround a surface containing air holes that are filled by a suitable analyte. This paper is aimed at designing an internal type PCF sensor with the analyte and multiple micrometer-sized holes in the middle. The different plasmonic materials are taken one by one and their properties are analyzed. The amplitude and wavelength sensitivities for each plasmonic material are calculated. The wavelength sensitivities for Silver, Gold, Aluminium, and copper are 1799nmRIU^{-1} , 1830.76nmRIU^{-1} , 1732nmRIU^{-1} and 1652nmRIU^{-1} respectively. For the Gold-Tin alloy, the calculated value of the Sensitivity in the wavelength measurement is 1532.2nmRIU^{-1} . The properties of these different sensors are then compared with each other. With the same set of chosen parameters, the best results are observed for Gold but the thickness of the gold film cannot be reduced below a few nanometers. Thus, in terms of stability and a wide range of parameters, silver has been observed to be the most suitable.

© 2023 Elsevier Ltd. All rights reserved.

Selection and peer-review under responsibility of the scientific committee of the International Conference on Materials and Manufacturing for Sustainable Developments – 2022.

1. Introduction

Biosensors have gained huge recognition over the last few years. The requirement of a biosensor is a tiny structure, remote sensing, and high sensitivity [1]. Biosensors are the sensors that sense the materials due to the biological or chemical reactions inside them due to the presence of an analyte. The analyte has the property of changing one of the parameters in the presence of a particular substance or radiations that need to be detected. The phenomenon observed after the fabrication of biosensors is Photoluminescence, Surface Plasmon Resonance Raman scattering, etc. The surface plasmon resonance is the most suitable phenomenon to work on because of its label-free detection. The first-ever surface plasmon resonance detection was performed by

Wood in 1902 [2]. In the experiment, a thin film of a plasmonic material was formed on top of a metal film. Then, using SPR, a small change in the refractive index of an organic material was observed after the absorption of the target gas. Additionally, the results were shown for a silicon glycol copolymer film of 430.8 angstrom thickness [2]. The film was exposed to different concentrations of the anesthetic gas halothane. The first-ever theoretical approach for SPR was implemented in 1950 by Ritchie [3]. The biosensors that are based on Surface Plasmon Resonance have the property of detecting the incident light due to changes in the refractive index of the analyte present. The analyte that is usually taken is silica. This type of biosensor has a wide range of applications in the field of pharmaceuticals and medical treatments. Traditionally, the SPR sensors had a prism-based structure and the light incident on the prism was further detected due to the variation of parameters like the refractive index. However, the complex and bulky structure of formerly designed SPR sensors led to the requirement of a rather compact structure. Then, the discovery of

* Corresponding author.

E-mail address: vinodsingh@dtu.ac.in (V. Singh).

¹ All the three authors contributed equally.

<https://doi.org/10.1016/j.matpr.2023.02.319>

2214-7853/© 2023 Elsevier Ltd. All rights reserved.

Selection and peer-review under responsibility of the scientific committee of the International Conference on Materials and Manufacturing for Sustainable Developments – 2022.

Please cite this article as: D. Kumar, M. Khurana, M. Sharma et al., Analogy of gold, silver, copper and aluminium based ultra-sensitive surface plasmon resonance photonic crystal fiber biosensors, Materials Today: Proceedings, <https://doi.org/10.1016/j.matpr.2023.02.319>

Photonic crystal fibers (PCF) led to a shift in the direction of SPR sensors [4,5]. PCF is superior in comparison to optical fibers in a way that they are micro-structured and use a constant refractive index of the cladding. The SPR-based biosensors using the PCF have an air holed- type structure with the substrate filled all around the air holes. Outside, the substrate surface, there is a thin nanofilm of a plasmonic material present. The molecules of the film get bound with the molecules of the analyte present outside the thin film. The mobile molecules of the analyte, on binding with the molecules of the plasmonic material reflect a change in the refractive index. The variation of refractive index with wavelength is linear and gives the confinement loss curve in a gaussian form. This curve is further used to determine the Sensitivity in the wavelength measurement and thus, the Sensitivity in the amplitude measurement [6,7]. The SPR sensors are categorized into two types, internal structured and external structured. The internal structured PCF has the substrate poured in between the air holes and the analyte surrounding the thin plasmonic material film, whereas in the externally structured PCF that delivers the external sensing, there is a formation of an analyte layer on the surface [8]. The most common plasmonic materials are Gold, Silver, Aluminium, and niobium which are used in the form of nanofilms. Silver has been observed to be the best material in this field. The reason for this material delivering great results is its properties like low optical damping and no interstate transitions [9]. Chao Liu et al performed a theoretical assessment on an SPR-based PCF sensor using gold as a plasmonic material. The spectral and amplitude sensitivities of the sensor were 5500 nm/RIU and 333.8 RIU⁻¹, respectively and the sensing resolution of the sensor was 7.69 × 10⁻⁶ RIU. The efficiency for the gold-based sensor was high because the thickness of the gold has been taken in a specified range [10]. On the other hand, aluminium forms a layer of Al₂O₃ when taken in the presence of oxygen. However, with unique properties, all these three types of plasmonic materials make the sensor an efficient one.

In this paper, we have taken a layer of silica at the outermost surface of the sensor with a comparatively thin layer of analyte present inside it. Then, there is a fabricated nanofilm of plasmonic material, with the substrate silica poured into the internal structure with multiple micro-sized air holes present inside to selectively vary the refractive index of the analyte. The thickness of the nanofilm taken is 40 nm. Through the Finite Element Meshing method, the structure has been fabricated and the parameters like wavelength, refractive index, thickness, and diameters of the various air holes have been varied and the confinement losses are thus calculated. Then, the confinement loss curves have been plotted. The Sensitivity in the amplitude measurement curves is also plotted with the main aim of differentiating between gold, silver, and aluminium-based sensors. The materials are differentiated by varying the material and plotting the parameters to get the sensitivities for the different plasmonic materials to get an idea of which material is the most suitable for the fabrication of biosensors in medical sensing applications.

2. Structural design and modelling

The designing of the model for the proposed sensors was initiated by forming a schematic structure first that represented the regions of the sensor having different materials as shown in Fig. 1. The selection of plasmonic materials has been made depending on the interaction of the electrons with the incident light on their surface. The substrate taken here is silica(SiO₂) which has been poured into the region between the holes and the outer surface. The analyte has been taken in the mentioned area and the function of the analyte is to act as a sticking agent between the mobile and immobile molecules. This action of the analyte causes

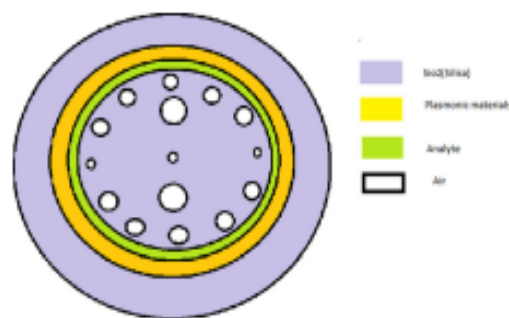


Fig. 1. Basic structural diagram for the proposed sensor.

a transition in the refractive index of the plasmonic material thin film taken. The interaction between the analyte and the incident light is functionalized by the layer of SiO₂. The radiations in the form of light are incident on the sensor's surface and its wavelength is detected due to the variation in the refractive index.

The Finite Element Method(FEM) is the mathematical key used with the help of COMSOL Multiphysics software version 5.6. The structure of the model has been designed as represented in Fig. 2. The cladding of the fiber has been designed in the form of air holes.

The specified values of the diameters of different regions have been taken to make the structure's functionality more efficient and have been presented in Fig. 2.

d_1, d_2, d_3 : The values for these parameters showing the diameter for the designed air holes are 400 nm, 0.8 μm and 1.6 μm respectively.

t_p : For the plasmonic material layer, the thickness is 40 nm.

t_a : For the analyte, the thickness is 2 μm.

n_a : The refractive index of the analyte with the value being 1.38.

λ : The wavelength of the incident light is, 0.6 μm.

The Drude- Lorentz model has been adopted to calculate the refractive index of silica [11,12,13].

From the model, the Sellmeier equation for SiO₂ can be given as:

$$n_{SiO_2}^2 = 1 + \frac{B_1 \lambda^2}{\lambda - C_1} + \frac{B_2 \lambda^2}{\lambda^2 - C_2} + \frac{B_3 \lambda^2}{\lambda^2 - C_3} \quad (1)$$

where $n_{SiO_2}^2$ represents the square of the refractive index of silica, λ is the wavelength(λ) in μm and $B_1, B_2, B_3, C_1, C_2, C_3$ are the Sellmeier coefficients [1].

Now, the confinement loss of the sensor can be calculated using the following equation [14],

$$\alpha_{con} = 8.856 \times \frac{2\pi}{\lambda} \times \text{Im}(n_{eff}) \times 10^4 \text{ dB/cm} \quad (2)$$

where λ is the wavelength(λ) in μm and $\text{Im}(n_{eff})$ is the imaginary part of the net effective refractive index.

There are two types of sensitivities of an SPR-based sensor, one is the sensitivity in wavelength measurement and the other is sensitivity in amplitude measurement.

For calculating the sensitivity in the wavelength measurement, the following equation is used, [15]

$$S_w(\lambda) = \frac{\Delta \lambda_{peak}}{\Delta n_a} \quad (3)$$

where $\Delta \lambda_{peak}$ is the variation of resonant curve peaks concerning the variation in the refractive indices, i.e., Δn_a .

For calculating the sensitivity in the amplitude measurement, the following equation is used, [16]

$$S_a(\lambda) = - \frac{1}{\alpha(\lambda, n_a)} \frac{\delta \alpha(\lambda, n_a)}{\delta n_a} \quad (4)$$

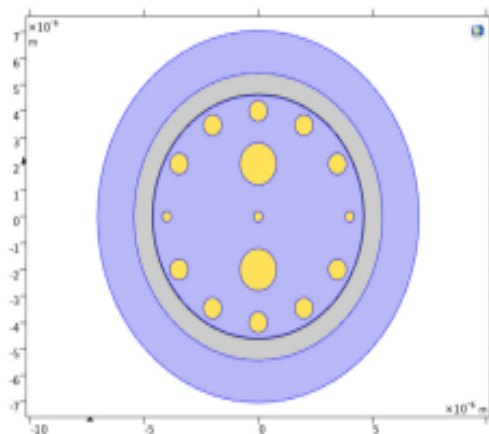


Fig. 2. Model structure in COMSOL.

Sensor resolution is defined as the smallest variation that is observed in the measurement of a parameter for specifying the sensor's activity. To measure the resolution of the sensor, the following equation is used [16],

$$R = \frac{\Delta n_s \Delta \lambda_{\min}}{\Delta \lambda_{\text{peak}}} \quad (5)$$

Here, Δn_s represents the variation in the refractive index, $\Delta \lambda_{\min}$ represents the minimum wavelength resolution and $\Delta \lambda_{\text{peak}}$ is the variation in the resonant wavelengths peak shift.

The figures, Fig. 3a and 3b represent the core modes of the sensor with the polarization in the x- and y- directions and the Surface Plasmon Polaritons modes of the sensor.

3. Results and discussions

After the successful structural designing of the model, the confinement losses and sensitivities are calculated for each material and thus plotted against the wavelength for varying refractive indices.

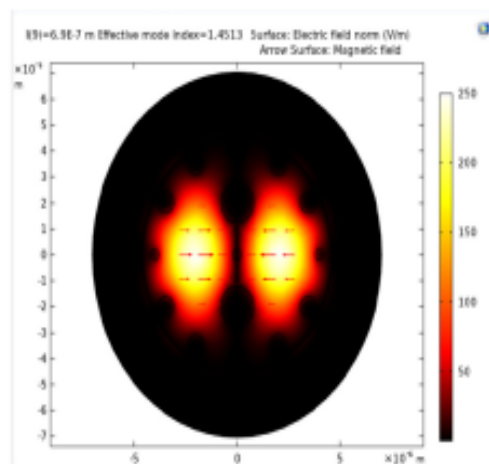


Fig. 3a. X-polarized core mode of the sensor.

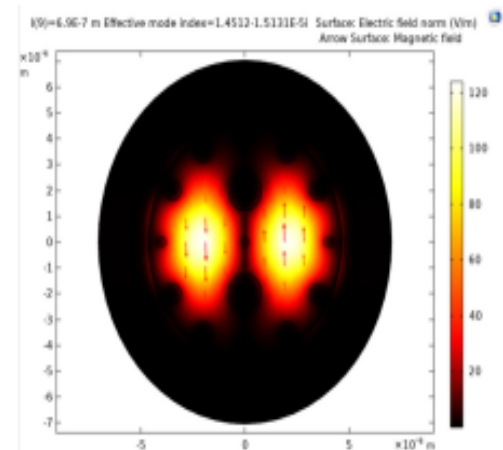


Fig. 3b. Y-polarized core mode of the sensor.

3.1. Phase matching

The core mode of the sensor contains the magnetic field lines in x- and y- directions inside the structure of the model whereas the SPP mode contains them at the boundary of the plasmonic material. The confinement loss of the sensor is calculated using equation (2) and thus, a graph is plotted against the wavelength for x- and y-polarizations respectively. Thus, the phase-matching curve (Figs. 4 and 5) is obtained and the peak value of the phase-matching wavelength is noted down.

The refractive indices are varied for lower ranges 1.25-1.30 with the materials being changed and the confinement losses are varied taking the wavelengths ranging from 0.5 to 0.65 μm . The following curves (Figs. 6 to 8) show the confinement loss curves for the calculation of Sensitivity in the wavelength measurement given by (3). For the gold nanofilm with a thickness of 40 nm, the following confinement loss curve is observed (Fig. 6).

For the silver nanofilm with thickness 40 nm, the following confinement loss curve is observed (Fig. 7).

For the aluminium nanofilm, copper nanofilm, and Au-tin alloy nanofilm with a thickness of 40 nm, the following confinement loss curve is observed in Figs. 8, 9, and 10 respectively. The sharper peaks are observed for aluminium and copper whereas the gold tin alloy curve has a rather flattened peak for confinement loss.

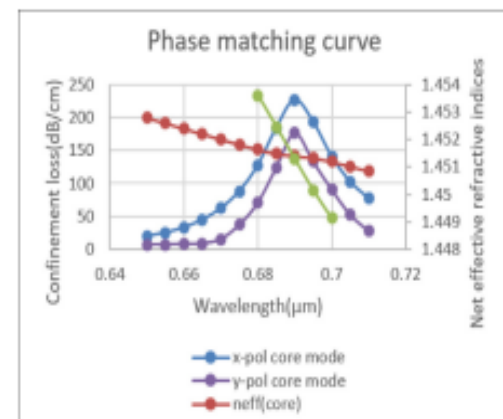


Fig. 4. Phase matching curve of core and SPP modes for gold nanofilm.

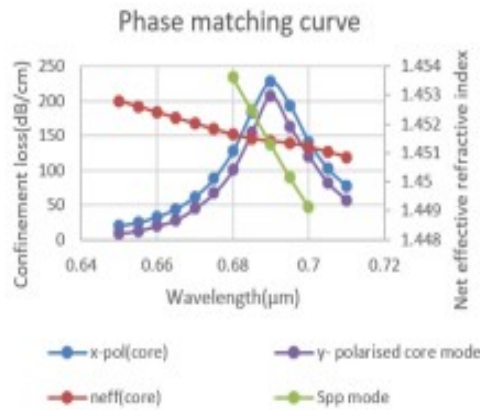


Fig. 5. Phase matching curve of core and SPP modes for silver nanofilm.

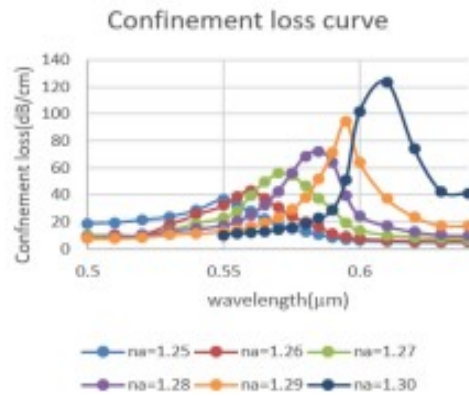


Fig. 6. Curve for the Confinement loss for gold nanofilm ($n_s = 1.25-1.30$).

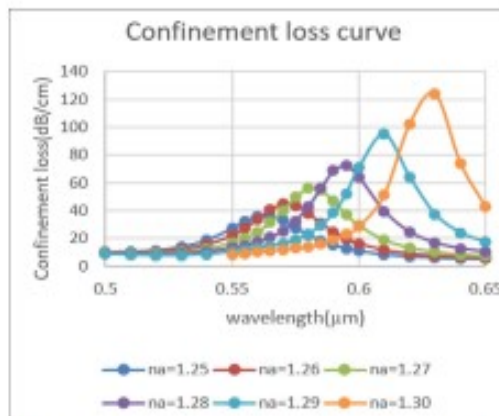


Fig. 7. Curve for the Confinement loss for silver nanofilm ($n_s = 1.25-1.30$).

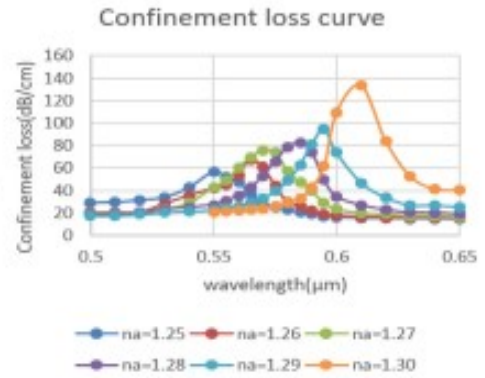


Fig. 8. Curve for the Confinement loss for aluminium nanofilm ($n_s = 1.25-1.30$).

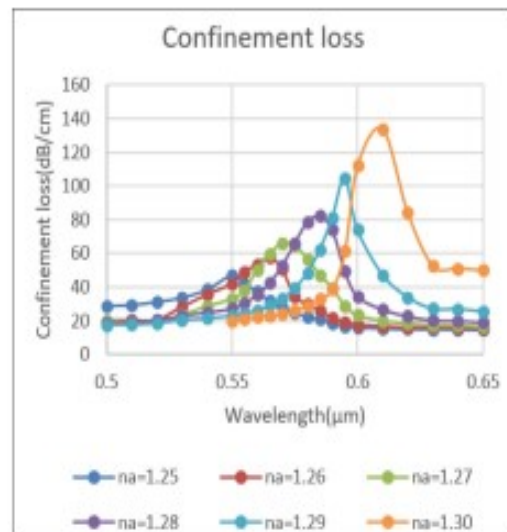


Fig. 9. Curve for the Confinement loss for copper nanofilm ($n_s = 1.25-1.30$).

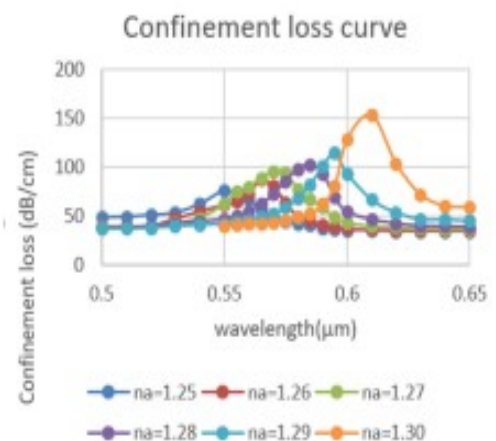


Fig. 10. Curve for the Confinement loss for gold-tin nanofilm ($n_s = 1.25-1.30$).

3.2. Calculation of wavelength sensitivities

The wavelength sensitivities for gold, silver, and aluminium nanofilm when the refractive indices are varied from $n_s = 1.25$ to $n_s = 1.30$ can be calculated from the confinement loss curves using equation (3).

The Table 1 for the observed values of $\Delta n_s (R2-R1)$ and $\Delta \lambda_{peak}$. Thus, the wavelength sensitivities of all three materials are of the same order, i.e., 10^3 nmRIU^{-1} .

3.3. Calculation of amplitude sensitivities

Calculating the amplitude sensitivities for each material for the refractive index varying from 1.25 to 1.30 and using equation (4), we have plotted the amplitude sensitivities against wavelength for the three materials. The amplitude thus calculated shows variation for different wavelengths as well as refractive indices. It is observed that as we increase the wavelength the Sensitivity in the amplitude measurement first increases slowly and then decreases sharply while for the larger refractive indices, higher peaks are observed as compared to that of the lower refractive

Table 1
Wavelength sensitivities for different materials.

Plasmonic material	$\Delta n_s (R2-R1)$	$\Delta \lambda_{peak}$	nmRIU^{-1}
Gold	0.05	91.538	1830.76
Silver	0.05	89.95	1799.00
Aluminium	0.05	86.61	1732.20
Copper	0.05	82.60	1652.00
Gold-tin	0.05	76.61	1532.2

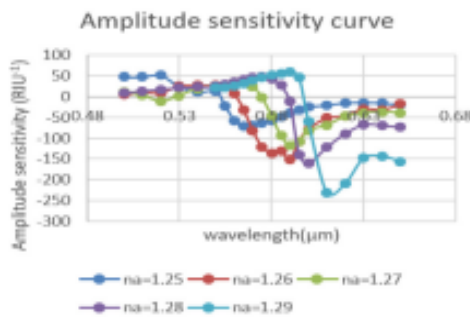


Fig. 11. Sensitivity in the amplitude measurement for gold nanofilm $n_s = 1.25-1.30$.

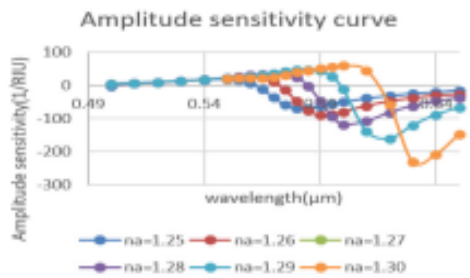


Fig. 12. Sensitivity in the amplitude measurement for silver nanofilm $n_s = 1.25-1.30$.

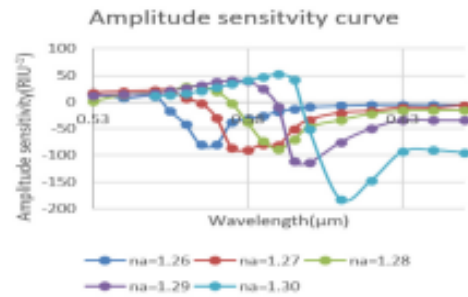


Fig. 13. Sensitivity in the amplitude measurement for aluminium nanofilm $n_s = 1.25-1.30$.

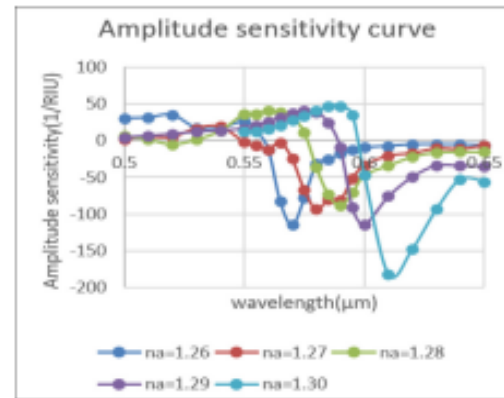


Fig. 14. Sensitivity in the amplitude measurement for copper nanofilm $n_s = 1.25-1.30$.

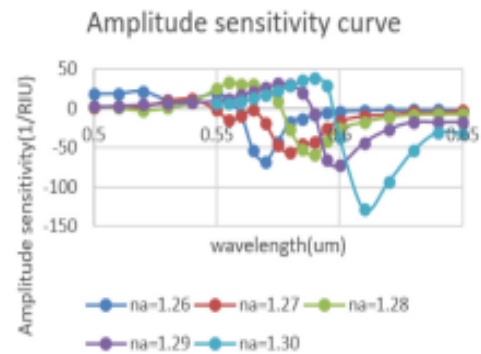


Fig. 15. Sensitivity in the amplitude measurement for gold-tin alloy nanofilm $n_s = 1.25-1.30$.

indices. Figs. 11 to 15 are showing the variation of Sensitivity in the amplitude measurement concerning the wavelength for different refractive indices for each plasmonic material.

The thus calculated amplitude sensitivities range is noted down and compared for each of the plasmonic materials. After comparing the amplitude sensitivities and the wavelength sensitivities, it is observed that the best results are obtained for the plasmonic material Gold followed by silver. Therefore, these materials are being

widely used. However, to make the sensor affordable and more compatible with good results, Aluminium nanofilm is recommended.

4. Conclusion

In this paper, we have designed an SPR-based PCF sensor with constant parameters like thickness, area, distance, and variable parameters like wavelength, refractive index, and plasmonic material. For different plasmonic materials, gold, silver, aluminium, copper, and gold-tin alloy. We have plotted the confinement loss curves and thus calculated the wavelength sensitivities. The maximum Sensitivity in the wavelength measurement is observed in the case of gold, i.e., 1830.76 nm/RIU, followed by silver, i.e., 1799 nm/RIU and then, there is the sensitivity of aluminium, i.e., 1732 nm/RIU. For copper, the Sensitivity in the wavelength measurement is 1652 nm/RIU and for the alloy of Gold and Tin, it is equal to 1532.2 nm/RIU. The amplitude sensitivities of the materials are plotted with a variation in wavelength and the finest curve can be seen in the case of silver nanofilm. The average resolution of the sensor is calculated to be of the order 10^{-5} . Thus, each material is suitable for effective sensing provided that an appropriate set of parameters are chosen. The SPR-based biosensors have a wide range of applications in biological and chemical analyte detection, medical diagnostics, food safety to security, and environmental monitoring.

CRedit authorship contribution statement

Deepak Kumar: Conceptualization, Methodology, Resources, Data curation, Writing – original draft. **Madhur Khurana:** Conceptualization, Methodology, Resources, Data curation. **Mukta Sharma:** Conceptualization, Methodology, Resources, Data curation, Writing – original draft. **Vinod Singh:** Conceptualization, Writing – review & editing, Investigation, Supervision.

Data availability

The authors are unable or have chosen not to specify which data has been used.

Declaration of Competing Interest

The authors declare that they have no known competing financial interests or personal relationships that could have appeared to influence the work reported in this paper.

Acknowledgement

We are thankful to Prof. Vinod Singh for guiding us through this project work.

References

- [1] N. Sabri, S.A. Aljunid, M.S. Salim, R.B. Ahmad, R. Kamaruddin, Toward optical sensors: review and applications, *J. Phys. Conf. Ser.* 423 (1) (2013), 012064. IOP Publishing.
- [2] B. Liedberg, C. Nylander, I. Lundström, Surface plasmon resonance for gas detection and biosensing, *Sens. Actuators* 4 (1983) 299–304.
- [3] J. Homola, Surface plasmon resonance sensors for detection of chemical and biological species, *Chem. Rev.* 108(2) (2008) 462–493, February 13.
- [4] Md. Rabul Hasan, Sanjida Akter, Kawsar Ahmed, Derek Abbott, Plasmonic Refractive Index Sensor Employing Niobium Nanofilm on Photonic Crystal Fiber, *IEEE Photonics Technol. Lett.* X(X), X 20XX.
- [5] Enramul Haque Sulaha Mahmuda Md. Anwar Hossain, Nguyen Hoang Hai, Highly Sensitive Dual-Core PCF Based Plasmonic Refractive Index Sensor for Low Refractive Index Detection, *IEEE Photon. J.* 11(5), October 2019.
- [6] Ahmed A. Rifat, Rajib Ahmed, G. Amouzad Mahdiraji, F.R. Mahamd Adikan, Highly Sensitive D-Shaped Photonic Crystal Fiber Based Plasmonic Biosensor in Visible to Near-IR, *IEEE Sens. J.* JSEN.2017.2677473.
- [7] Tanvir Alam Roni, Rifat Hassan, Mohammad Faisal, Dual-Side Polished SPR Biosensor with Wide Sensing Range, 2020 11th International Conference on Electrical and Computer Engineering (ICECE).
- [8] Lu Junjie, Y. Li, Y. Han, Y.L. Liu, J. Gan, D-shaped photonic crystal fiber plasmonic refractive index sensor based on gold grating, *Appl. Opt.* 57 (19) (July 2018) 1.
- [9] E. Kretschmann, H. Raether, Radiative Decay of Non Radiative Surface Plasmons Excited by Light, *Notizen, (Z. Naturforsch.* 23 a, 2135–2136 [1968].
- [10] C. Liu, L. Yang, Lu, Xili, Q. Liu, F. Wang, L.V. Jingwei, T. Sun, Mid-infrared surface plasmon resonance sensor based on photonic crystal fibers, *Opt. Express* 25 (13) (2017).
- [11] Singh, V., Kumar, D., Sharma, M., Surface Plasmon Resonance implemented silver thin film PCF sensor with multiple-Hole microstructure for wide ranged refractive index detection, *Mater. Today Proc.* 62(Part 12) (2022) 6590–6595.
- [12] Pier J.A. Sazio, et al., Reactors Microstructured Optical Fibers as High-Pressure Microfluidic reactors, *Science* 311, 1583(2006).
- [13] Alexandre Vial,* Anne-Sophie Grimaud, Demetrio Macías, Dominique Barchiesi, Marc Lamy de la Chapelle, Improved analytical fit of gold dispersion: Application to the modeling of extinction spectra with a finite-difference time-domain method, *Phys. Rev. B* 71, 085416 s2005d.
- [14] V. Singh, D. Kumar, M. Sharma, Gold/ZnO Interface-Based D-Shaped PCF Surface Plasmon Resonance Sensor with Micro-Openings, *Analytic Designing and Some Applications*, in: K. Goetha, F.M. Gonzalez-Longatt, H.M. Wee (Eds.), *Recent Trends in Materials*. Springer Proceedings in Materials, vol 18, Springer, Singapore, 2022, https://doi.org/10.1007/978-981-19-5395-8_27.
- [15] C. Liu, S.u. Weiguan, Q. Liu, Lu, Xili, F. Wang, T. Sun, P.K. Chu, Symmetrical dual D-shape photonic crystal fibers for surface plasmon resonance sensing, *Opt. Express* 26 (7) (2018).
- [16] Markus Hautakorpi, Maija Mattinen, Hanne Ludvigsen, Surface-plasmon-resonance sensor based on three-hole microstructured optical fiber, 060.2280) Fiber design and fabrication; (060.2340) Fiber optics components; (240.6680) Surface plasmons.